Available online at www.sciencedirect.com
ScienceDirect
Wear 263 (2007) 1397–1416
WEAR
www.elsevier.com/locate/wear

Microstructural and tribological comparison of HVOF-sprayed and post-treated M–Mo–Cr–Si (M = Co, Ni) alloy coatings

Giovanni Bolelli [a,*], Valeria Cannillo [a], Luca Lusvarghi [a], Monia Montorsi [a], Fabio Pighetti Mantini [a], Massimiliano Barletta [b]

[a] *Dipartimento di Ingegneria dei Materiali e dell'Ambiente, University of Modena and Reggio Emilia, Via Vignolese 905, 41100 Modena, Italy*
[b] *Dipartimento di Ingegneria Meccanica, University of Rome "Tor Vergata", Via del Politecnico 1, 00133 Rome, Italy*

Received 11 August 2006; received in revised form 7 December 2006; accepted 9 December 2006
Available online 13 March 2007

Abstract

High velocity oxygen-fuel (HVOF)-sprayed wear resistant Co–28%Mo–17%Cr–3%Si and Ni–32%Mo–15%Cr–3%Si coatings, both as-sprayed and after heat treatments at 600 °C for 1 h, have been studied. Particularly, their dry sliding wear behaviour has been compared by ball-on-disk tests against different counterbodies (100Cr6 steel and sintered alumina), and differences were discussed based on microstructural characteristics and micromechanical properties (Vickers microindentation and scratch test responses). As-sprayed coatings contain oxide stringers, are mostly amorphous and display rather low Vickers microhardness (about 7.4 GPa for the Co-based and 6.2 GPa for the Ni-based), toughness and elastic modulus. Heat-treated ones display sub-micrometric crystalline intermetallics, improving hardness (9.6 GPa and 7.4 GPa, respectively) and elastic modulus. Scratch tests indicate greater brittleness of the Ni-based alloy (higher tendency to cracking). Due to low hardness and toughness, both as-sprayed coatings undergo wear loss against steel and alumina counterparts. The more plastic Co-based alloy undergoes higher adhesive wear against steel and lower abrasive wear against alumina; the situation is reversed for the Ni-based alloy. After heat treatment, the wear loss against steel is very low for both coatings; abrasive wear still occurs against alumina.

Keywords: Co alloy; Ni alloy; HVOF spraying; Pin-on-disk test; Sliding wear; Post-treatment

1. Introduction

Thermal spraying is a common family of hardfacing techniques, which, compared to other processes (like welding techniques), are characterized by flexibility in coating material choice, low substrate thermal input and virtually no substrate dissolution [1]. In particular, high velocity oxygen-fuel (HVOF) flame spraying produces dense coatings with no interconnected porosity, low degree of oxidation and high adhesion strength [1–3].

Among available hardfacing materials, alloys belonging to the Tribaloy®[1] family, with general composition M–Mo–Cr–Si (M = Co or Ni), are particularly interesting, since they are strengthened by peculiar Laves phases. They are topologically close packed intermetallic phases, with M–Mo or M–Mo–Si based composition [4,5]. Their particular close-packed structure hinders dislocation movement [4], making them very hard, but also rather brittle [4–6]. Therefore, Tribaloys are seldom employed in bulk form, but rather applied as wear resistant coatings [7–11]. Since purely metallic Laves phases are less hard than carbides [5,11], Tribaloy coatings are often reported to display lower wear resistance than carbide-containing coatings, like thermally sprayed or clad cermets [11–13]. Nonetheless, the high hardness of carbides also implies some disadvantages: carbide-based coatings are more difficult to grind and polish and they may inflict high counterpart wear [5,11,12]. Moreover, in thermal spray processes, cermet powders are often more expensive and display lower deposition efficiency than metallic ones [14].

Thus, investigation on the wear resistance of HVOF-sprayed Tribaloy-based coatings is of technological interest. Moreover, in literature, much more knowledge exists on the characteristics of welded or laser-clad Tribaloys [7–9] than thermally sprayed

* Corresponding author. Tel.: +39 059 2056206; fax: +39 059 2056243.
E-mail address: bolelli.giovanni@unimore.it (G. Bolelli).
[1] Trademark of Deloro Stellite.

0043-1648/$ – see front matter © 2007 Elsevier B.V. All rights reserved.
doi:10.1016/j.wear.2006.12.002

ones [10,11], and HVOF-sprayed in particular [12,13,15–18]. The microstructure of HVOF-sprayed Tribaloy coatings is significantly different from that of clad or welded ones, due to the peculiarities of HVOF-spraying. Welded Tribaloys display a fully crystalline microstructure resulting from melt solidification. In the case of hyper-eutectic compositions, like Tribaloy-800 (Co–28 wt.%Mo–17 wt.%Cr–3 wt.%Si) and Tribaloy-700 (Ni–32 wt.%Mo–15 wt.%Cr–3 wt.%Si), primary Laves-phase dendrites are formed in an eutectic matrix comprising fine Laves-phase and Co- or Ni-based solid solution lamellar crystals [6–8]. In HVOF-sprayed Tribaloy coatings, first of all, the high velocity impact of heated particles generates a layered lamellar microstructure, like every thermally sprayed material. Besides, the cooling rate of each heated particle upon impact is extremely high (>10^5 K/s), causing splat quenching: this results in very fine submicrometric crystals, metastable supersaturated solid solutions, and even amorphous phases within each splat [13,15,18]. Therefore, knowledge acquired for welded or clad Tribaloys cannot be directly transferred to HVOF-sprayed coatings, which require specific research. A former study by the authors showed that as-deposited HVOF-sprayed Tribaloy-800 coatings display low mechanical properties due to a largely amorphous as-quenched intrasplat structure, resulting in severe adhesive wear in dry sliding against a steel counterpart. Instead, a proper thermal treatment at 600 °C for 1 h favours the precipitation of small, sub-micrometric crystals definitely enhancing mechanical properties and thus improving the dry sliding wear resistance against steel by several orders of magnitude [18].

The objective of the present research is to extend the tribological study presented in [18]. A wider range of dry sliding contact conditions is tested and, most importantly, the wear behaviour of the formerly considered Co-based Tribaloy-800 coating is compared to the Ni-based Tribaloy-700. Indeed, systematic comparisons of the properties and wear behaviour of Tribaloy-700 and Tribaloy-800 are very scarce in literature (some comparison is only found in ref. [11]) and not provided for HVOF-sprayed coatings. The two alloys have similar content of alloying elements (Mo, Cr, Si); the Tribaloy-700 is described as an alternative to the Tribaloy-800 for nuclear applications [19,20]. Therefore, it is interesting to highlight differences in their tribological behaviour in order to provide industrial designers with a basis for coatings choice. The effect of the 600 °C-heat treatment, introduced in [18], will be investigated in this study as well. A correlation between tribological behaviour and micromechanical properties will be sought for.

2. Materials and characterization

A Co–28%Mo–17%Cr–3%Si powder, with composition analogous to Tribaloy-800® (Praxair Co-111, gas atomised, −45 + 10 μm), and a Ni–32%Mo–15%Cr–3%Si powder (all compositions in weight percentage), with composition analogous to Tribaloy-700® (Sandvik-Osprey Ni700, gas atomised, −53 + 10 μm) were thermally sprayed onto C40 (=AISI 1040) steel plates (100 mm × 100 mm × 5 mm) by a Praxair-Tafa JP5000 HVOF torch[2], with spray parameters listed in Table 1. Steel plates were grit-blasted with 500 mesh alumina particles using a hand-held vacuum operated blasting gun immediately before coating deposition. Substrate temperature was monitored during spraying by a thermocouple in contact with the plate back side and was kept below 200 °C. The two coatings will be briefly referred to as Co800 (Tribaloy-800) and Ni700 (Tribaloy-700).

Table 1
JP5000 spray parameters for both spray powders

Parameter	Value
Barrel length (mm)	102
O_2 flux (Sl/min)	920
Kerosene flux (l/min)	0.379
Powder carrier gas (Sl/min)	10.5
Feeding disk revolution speed (rpm)	270
Spray distance (mm)	380
Gun traverse speed (mm/min)	500

The as-supplied spray powders were characterized by thermogravimetric analysis (TG, Perkin Elmer TGA 7) and differential thermal analysis (DTA, DTA 404, Netzsch, Selb, Germany) in air (10 °C/min heating rate up to 1300 °C) in order to investigate their reactivity with oxygen. To examine the transformations occurring at each DTA peak, powders were heat treated in air at the respective peak temperature for 5 min (10 °C/min heating rate) and were then observed by scanning electron microscope (SEM, XL-30 and Quanta-200, FEI, Eindhoven, The Netherlands).

Coatings were characterized both in the as-deposited condition and after heat treatment at 600 °C for 1 h in an electric kiln in air (15 °C/min heating rate, sample cooling inside the kiln).

Polished cross-sections (mounted in resin) were observed by SEM and employed for depth-sensing microindentation (Depth-Sensing Vickers Microindenter, C.S.M. Instruments, Peseux, Switzerland). 1 N (≈100 g) load was used for Vickers microhardness evaluation (optical indentation diagonal measurement) and elastic modulus measurement (Oliver-Pharr procedure [21], 0.8 N/min loading and unloading rates, 15 s loading time, Poisson's ratio assumed equal to 0.30), 5 N for indentation fracture toughness. The microcracks produced by the indentation are measured by optical microscopy. The Evans and Wilshaw formula [22] is employed for toughness calculation (1):

$$K_{Ic} = 0.079 \frac{L}{a^{3/2}} \log\left(\frac{4.5a}{c}\right) \quad (1)$$

where L is the indentation load (mN); a the indentation half-diagonal (μm); c is the average crack length, measured from the indentation centre (μm); K_{Ic} is the indentation fracture toughness (MPa $m^{1/2}$).

Since in thermally sprayed coatings cracks preferentially propagate along interlamellar boundaries, it is often found that cracks normally range out from the indentation diagonal parallel to the substrate interface but not from the one perpendicular to the interface. The computation technique described in [23] is employed to account for this phenomenon.

[2] Owned by Centro Sviluppo Materiali S.p.A., Roma, Italy.

X-ray diffractometry (XRD, X'pert Pro diffractometer, PANalytical, Eihndoven, The Netherlands, using Cu Kα1 radiation) was performed on the supplied spray powders and on polished surfaces. In order to compare the crystal grain size in as-sprayed and heat-treated coatings, the full width at half-maximum height (FWHM) has been computed for the more clearly distinguishable diffraction peaks, and the grain size of the various phases has been subsequently estimated by applying the Sherrer formula [24] (2).

$$d = \frac{0.94\lambda}{W\cos\theta} \quad (2)$$

where λ is the X-ray wavelength = 1.54060 Å (Cu Kα1 radiation); W the full peak width at half-maximum height (FWHM) (rad); θ is the incidence angle.

The ratio between the estimated grain sizes for as-sprayed and heat treated coatings has thus been computed. To test the consistency of the method, the formula was applied to more than one peak for each phase (when possible), in order to check if similar ratios are obtained in all cases. For FWHM calculation, preliminary diffraction pattern smoothing and background subtraction were performed using the Powder4 software [25].

A better quantitative estimation of the average grain size has been obtained by applying image analysis techniques (ImageJ version 1.34, NIH) on high-resolution field emission gun-SEM micrographs (FEG-SEM, Leo Supra 35) taken on polished coating surfaces (ground with 400, 800, 1000, 2000 mesh SiC papers and polished with Al_2O_3 slurry down to 0.3 μm grain size).

Polished coating surfaces (ground with 400, 800, 1000 mesh SiC papers and 10 μm and 5 μm diamond papers; Ra ≈ 0.5 μm) were subjected to scratch test using Rockwell conical diamond stylus with 200 μm tip radius (Micro-scratch tester, C.S.M. Instruments). Two scratches in "progressive" mode, i.e. with linearly increasing load (0.1–30 N, 5 mm length, 5 N/min loading rate), and a "multi-pass" mode scratch test, i.e. four passes over the same track (10 N load, 5 mm length, 0.84 mm/min scratch speed) were performed on both as-sprayed and heat treated Tribaloy-700 and 800 coatings. Scratch tracks were visually inspected by optical microscope and SEM and their 3D profiles were acquired (non-contact optical confocal profilometry; Conscan Profilometer, C.S.M. Instruments).

Rotating unidirectional ball-on-disk dry sliding tribological tests were performed on polished samples with a pin-on-disk tribometer (C.S.M. Instruments) against 100Cr6 balls (nominal hardness HV = 7 GPa) and sintered alumina balls (nominal hardness HV = 19 GPa). Test conditions are listed in Table 2. The radius between the pin position and the sample revolution axis is fixed at 5 mm. Sample wear rate was calculated by measuring the average cross-sectional area of the wear track by optical profilometry (Conscan profilometer), computing the resulting wear volume. The friction coefficient is monitored on-line during the test.

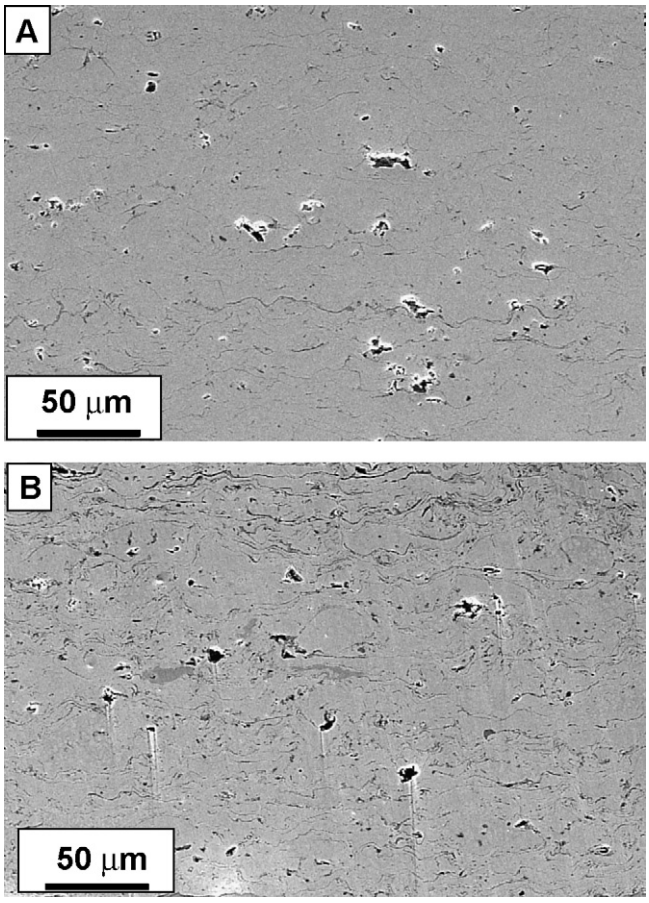

Fig. 1. Cross-sections of as-sprayed Co800 (A) and Ni700 (B).

3. Results

3.1. Coatings structure and microstructure

Both as-deposited coatings display some closed porosity and some unmelted or partially melted particles with quite rounded morphology. Some oxide inclusions, mainly splat-boundary oxide stringers, are also recognizable as small dark grey areas in SEM micrographs, and are more abundant in the Ni700 coating than in the Co800 one (Fig. 1A and B). Large micron-sized

Table 2
Pin-on-disk test conditions

	Test 1	Test 2	Test 3	Test 4	Test 5	Test 6	Test 7	Test 8
Ball material	100Cr6 steel	100Cr6 steel	100Cr6 steel	100Cr6 steel	Sintered Al_2O_3	Sintered Al_2O_3	Sintered Al_2O_3	Sintered Al_2O_3
Ball diameter (mm)	6	6	3	3	6	6	3	3
Normal load (N)	5	10	5	10	5	10	5	10
Sliding speed (m/s)	0.2	0.2	0.2	0.2	0.2	0.2	0.2	0.2
Sliding distance (m)	500	500	500	500	500	500	500	500

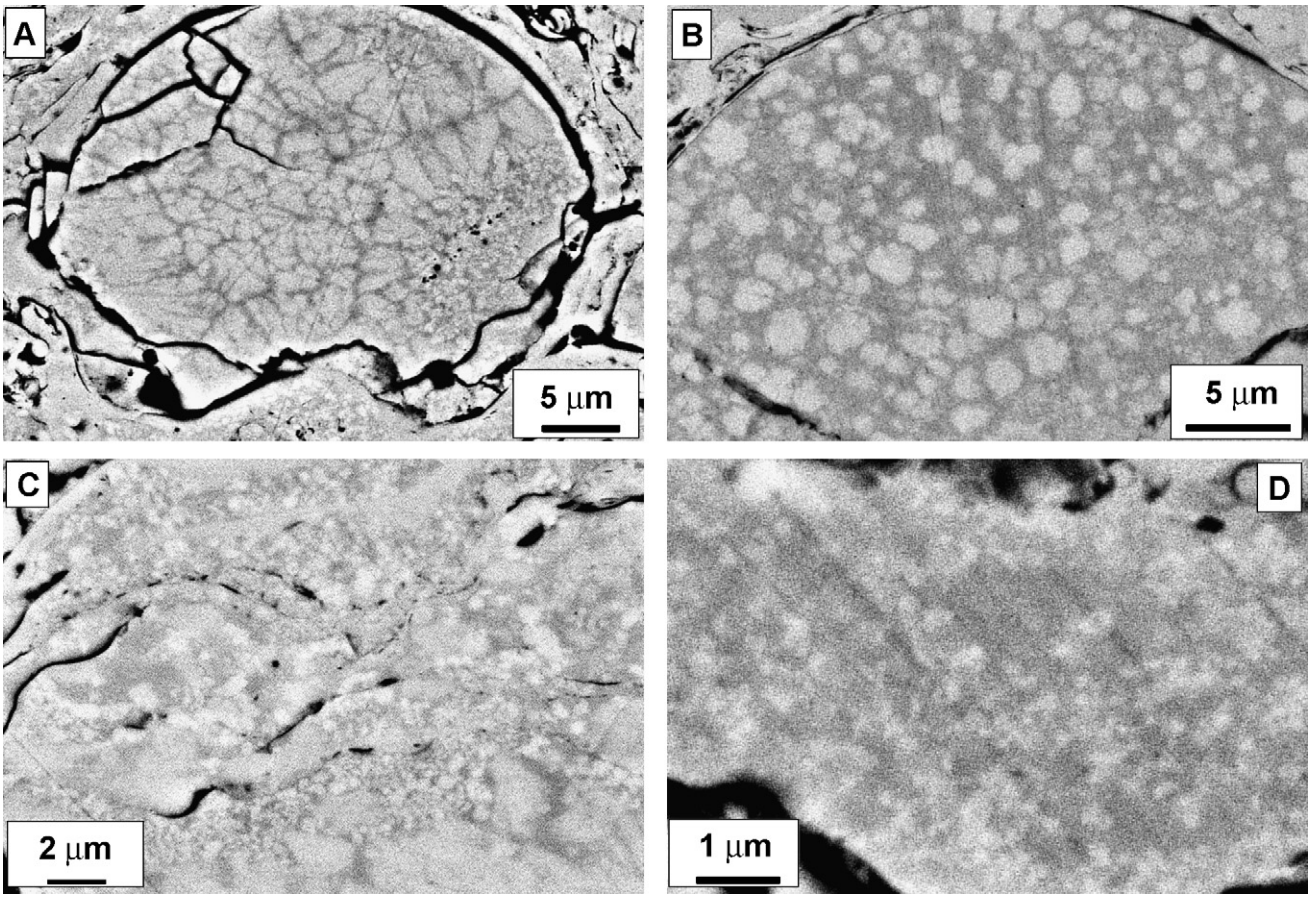

Fig. 2. Detailed cross-sectional SEM micrographs of coatings. (A and B) Detail of unmelted particles in Co800 (A) and Ni700 (B) coatings, showing large micron-sized grains. (C and D) Detail of heat-treated Co800 (C) and Ni700 (D) coatings, showing small sub-micrometric grains.

grains (brighter than the surrounding matrix in backscattered electron imaging) are present in rounded unmelted or partially melted particles, and sometimes display a dendritic morphology (Fig. 2A and B). EDS microanalysis indicates that these grains are, in all cases, richer in Mo and Si and poorer in Cr than the matrix. Instead, most fully melted, flattened lamellae display a homogeneous microstructure with no clearly perceivable secondary precipitates. After the heat treatment, the porosity, the lamellar microstructure, the oxide inclusions amount and morphology do not significantly change for both materials. However, inside the splats, a large number of very small (sub-micrometric) grains appear in high-magnification images (Fig. 2C and D).

XRD patterns indicate that, while spray powders display sharp diffraction peaks, the as-sprayed coatings possess broad diffraction peaks and exhibit an amorphous hump at $40° < 2\theta < 50°$. Several crystalline phases are identifiable. Particularly, the Co800 coating contains Co_7Mo_6, Co_3Mo_2Si, $CoSi_2$ and a Co–Mo–Cr solid solution with fcc lattice (Fig. 3A). The Ni700 contains a Ni-based fcc solid solution, Mo_5Si_3, Ni_3Si_2 and Mo (Fig. 3B). After the heat treatment, more intense and clearly distinguishable peaks appear, but diffraction peaks are still significantly broad. The ratio between the crystal grain size in as-sprayed and heat treated coatings has been estimated from diffraction peak width using the Sherrer formula (2), both for Co800 and for Ni700 (Table 3). In most cases, the ratio is close

Table 3
Full width at half-maximum height (FWHM) for some diffraction peaks in as-sprayed and heat-treated coatings, and ratio between corresponding grain sizes as estimated by Sherrer formula (2)

Material	Phase	Position (2θ)-AS	FWHM-AS	Position (2θ)-HT	FWHM-HT	HT/AS
Co800	Co_3Mo_2Si	38.066	0.46944	38.24054	0.51274	0.92
Co800	Co_3Mo_2Si	41.55073	0.3396	41.70518	0.29768	1.14
Co800	Co_3Mo_2Si	45.01312	0.37725	45.14693	0.31528	1.20
Co800	Co_7Mo_6	43.37324	0.79095	42.62499	0.51881	1.52
Ni700	Mo_5Si_3	38.06223	0.46868	38.15232	0.31993	1.47
Ni700	Ni-s.s.	50.18186	0.84612	50.59222	0.90284	0.94
Ni700	Ni-s.s.	73.80599	1.11441	74.32006	1.40775	0.79

AS: as-sprayed; HT: heat-treated; HT/AS: estimated grain size ratio between heat-treated and as-sprayed coatings.

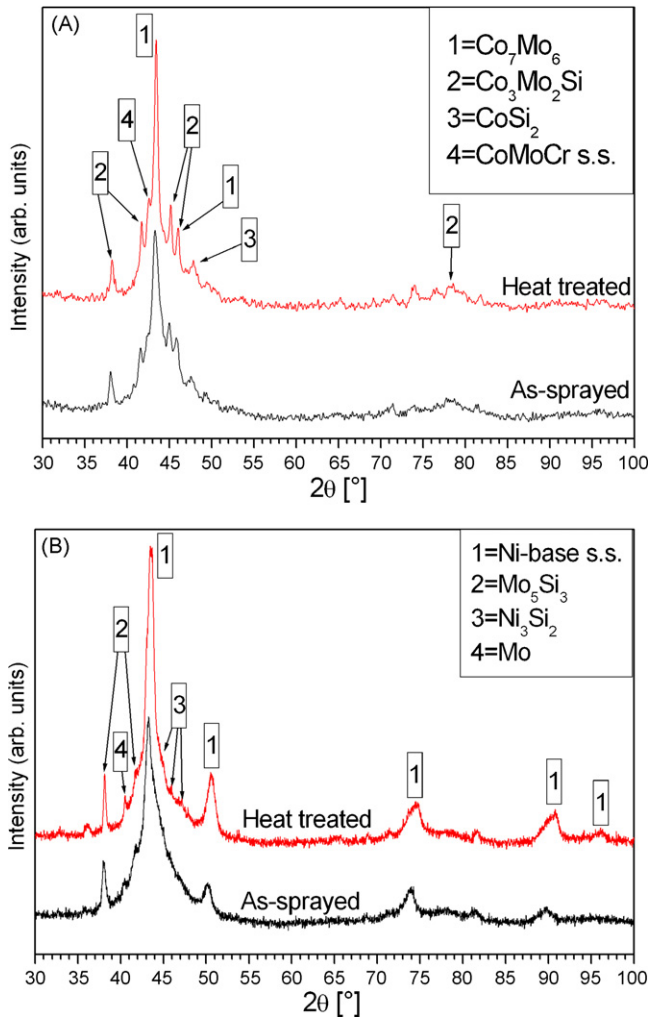

Fig. 3. X-ray diffraction pattern for as-sprayed and heat treated Co800 (A) and Ni700 (B) coatings. *Note*: s.s. = solid solution.

Table 4
Average grain size of precipitates found in fully melted splats

Coating	Average grain size (nm)
Ni700 (as-sprayed)	89 ± 35
Ni700 (heat treated)	146 ± 48
Co800 (as-sprayed)	185 ± 91
Co800 (heat treated)	199 ± 116

to unity. Values obtained by applying the formula to different peaks belonging to the same phase are quite similar, confirming the consistency of the method.

High-resolution FEG-SEM (Fig. 4A–D) micrographs give a better insight into the microstructure of fully melted lamellae, where very small crystalline grains appear. The average size of the precipitates appearing in those areas is reported in Table 4 for as-sprayed and heat treated coatings. Much larger grains appearing in partially or totally unmolten particles embedded in the coating have not been considered in this computation.

3.2. DTA-TG analysis

Co800 powder exhibits three exothermal DTA peaks at 846 °C, 1050 °C and 1146 °C, with reaction onset around 700 °C and 40% weight gain up to 1300 °C (from TG). The Ni700 powder has one exothermal DTA peak at 1258 °C, onset around 860 °C and 15% weight increase up to 1300 °C.

Co800 powder treated isothermally at 846 °C for 5 min displays a very fine grained oxide layer (average grain size around 100 nm, Fig. 5A). Significant fluctuations (large standard deviation) exist in the average chemical composition as determined by EDS microanalysis on different points of this layer. After the 1050 °C, 5 min heat treatment on the powder, slightly larger grains appear (Fig. 5B), containing only Cr and O (Table 5). After the 1146 °C treatment, the surface morphology is significantly altered (Fig. 5C). Large oxidized areas containing all coating constituents (Table 5) are scattered throughout the surface (labelled as 1); the surrounding surface (labelled as 2) seems damaged, with large pores, and contains much less oxygen (Table 5).

Ni700 powder treated at 1258 °C is covered by a large-grained oxide layer (Fig. 5D). EDS microanalysis (Table 5) indicates the presence of Ni, Cr, O in the smaller grains (labelled as 1), while in the larger ones (labelled as 2) almost only Ni and O are found (with very minor amounts of Cr).

3.3. Micromechanical properties

As-sprayed coatings possess significantly lower microhardness and elastic modulus compared to 600 °C-heat treated ones; indentation fracture toughness, instead, does not improve significantly (Table 6). Fig. 6A and B display optical micrographs of 5 N indentation marks: cracks often propagate along splat boundaries, in the direction parallel to the substrate interface.

Table 5
Semi-quantitative chemical composition (in weight %, normalized to 100%) of oxide layers on spray powders heat treated at the various DTA peaks (5 min isotherm time), obtained by EDS analysis

Sample	Co800 846 °C	Co800 1050 °C	Co800 1146 °C area 1	Co800 1146 °C area 2	Ni700 1258 °C area 1	Ni700 1258 °C area 2
Co%	21.82 ± 8.03	3.56 ± 1.76	27.43 ± 3.69	38.37 ± 2.35	–	–
Ni%	–	–	–	–	25.66 ± 5.93	57.28 ± 1.75
Cr%	25.23 ± 8.56	51.38 ± 4.65	11.59 ± 0.19	14.54 ± 0.47	29.59 ± 6.17	5.16 ± 1.60
Mo%	14.28 ± 6.69	0	23.98 ± 0.59	27.20 ± 3.67	0	0
Si%	2.15 ± 0.75	0	3.21 ± 0.28	3.29 ± 0.09	0.41 ± 0.57	0
O%	36.52 ± 9.39	51.38 ± 14.79	33.80 ± 2.64	16.62 ± 0.94	44.35 ± 0.34	37.57 ± 0.15

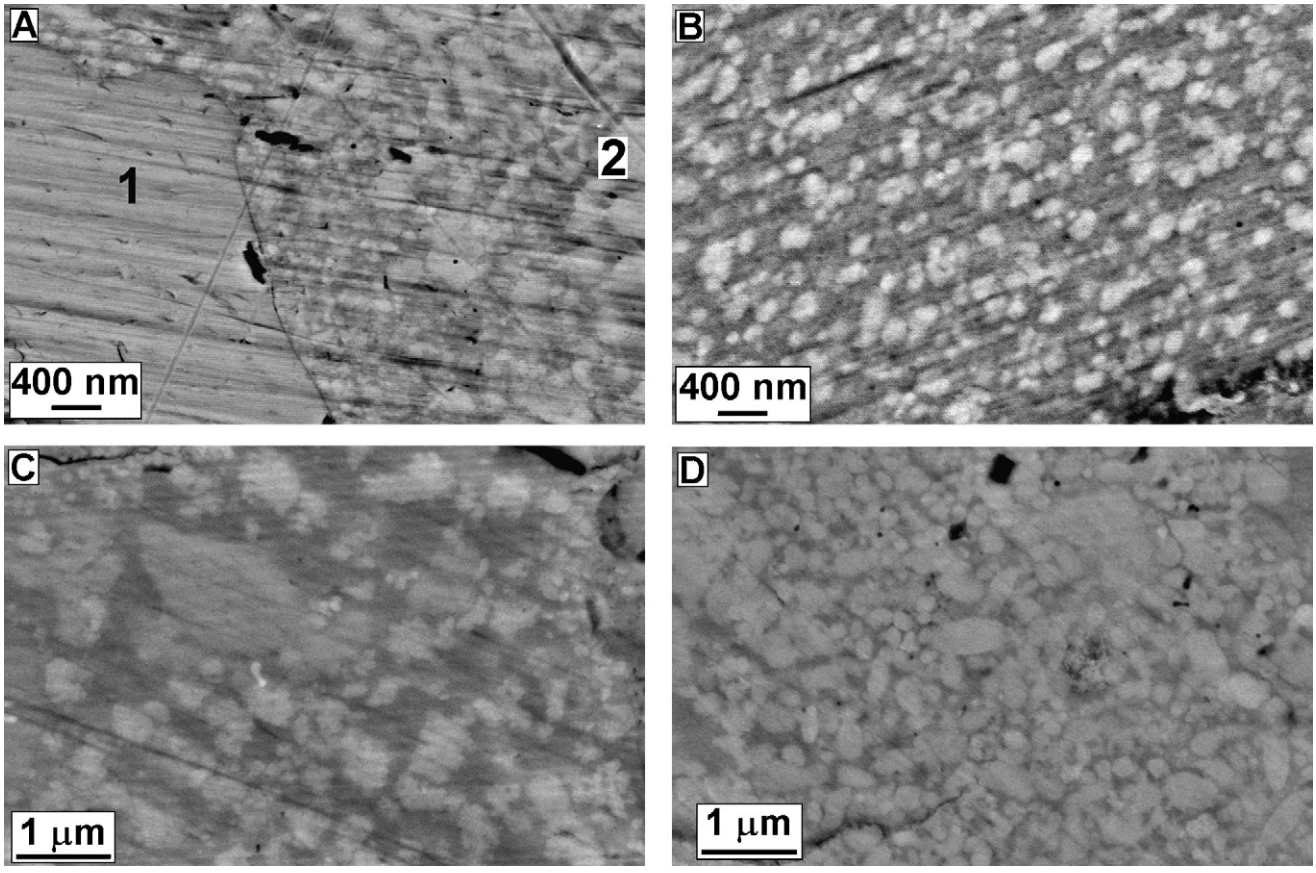

Fig. 4. High-resolution FEG-SEM micrographs of coatings: (A) Ni700 as-sprayed (1 = region with no visible precipitates; 2 = region with sub-micrometric precipitates); (B) Ni700 heat treated; (C) Co800 as-sprayed; (D) Co800 heat treated.

At the edges of the diagonal perpendicular to the substrate interface, there may be no cracking (Fig. 6A). In other cases, defects (like unmolten particles) trigger multiple cracking, or result in cracks not originating from the diagonal edge (Fig. 6B). If a 10 N load is employed, crushing and collapsing of material under the indenter may occur, making toughness measurement not possible (Fig. 6C).

From "progressive" scratch tests, the critical load for the appearance of the first crack (Lc1) and of the first track side chipping (Lc2) can be found (Table 7). Both values increase passing from Ni700 to Co800 coatings, and significantly increase from as-sprayed to heat treated coatings (Lc2 in particular). When indentation load exceeds Lc1, as-sprayed Co800 coating displays a rather low degree of cracking (Fig. 7A) until load reaches quite high values. Larger damage beyond Lc1 is observed in as-sprayed Ni700, where evidence of a certain tendency to delamination is also noticeable (Fig. 7B). In heat-treated Ni700, tendency to delamination is slightly lower (Fig. 7C). While in all other coatings cracks seem to follow a rather irregular pattern, in heat-treated Co800 coatings they tend to follow more regular, near semi-circular paths. In this coating, cracks start from the groove side at Lc1 and then extend to the groove centre when load increases, forming complete semi-circular transverse cracks (Fig. 7D).

Table 6
Depth-sensing Vickers microindentation test results

Coating	$HV_{0.1}$ (GPa)	E (GPa)	K_{Ic} (MPa $m^{1/2}$)
Co800 (as-sprayed)	7.40 ± 0.81	169.5 ± 5.8	1.391 ± 0.337
Ni700 (as-sprayed)	6.21 ± 0.70	148.5 ± 17.5	1.906 ± 0.803
Co800 (heat-treated)	9.65 ± 0.91	292.9 ± 18.7	1.521 ± 0.475
Ni700 (heat-treated)	7.40 ± 1.50	260.7 ± 12.0	1.437 ± 0.551

3D profile measurements of "multi-pass" scratch tests allow the determination of the average cross-sectional profile of the scratch track. The average cross-sectional area of the groove (A_g), the average area of the side pile-up (A_p), and A_p/A_g ratio can be computed. The as-sprayed Co800 displays a lower groove cross-sectional area, but a higher pile-up/groove area ratio than as-sprayed Ni700 (Table 7): in the former coating, a greater percentage of the material originally placed in the groove position has been displaced to the side, while more material loss took place in the latter. The A_p/A_g ratio decreases after thermal treatment, but the ranking between Co800 and Ni700 remains the same.

3.4. Ball-on-disk tests

Among as-sprayed coatings, Co800 performs definitely worse than Ni700 against 100Cr6 steel counterparts, wear rates being always at least five times greater (Fig. 8). The ranking, however, is completely reversed with Al_2O_3 counterpart. With

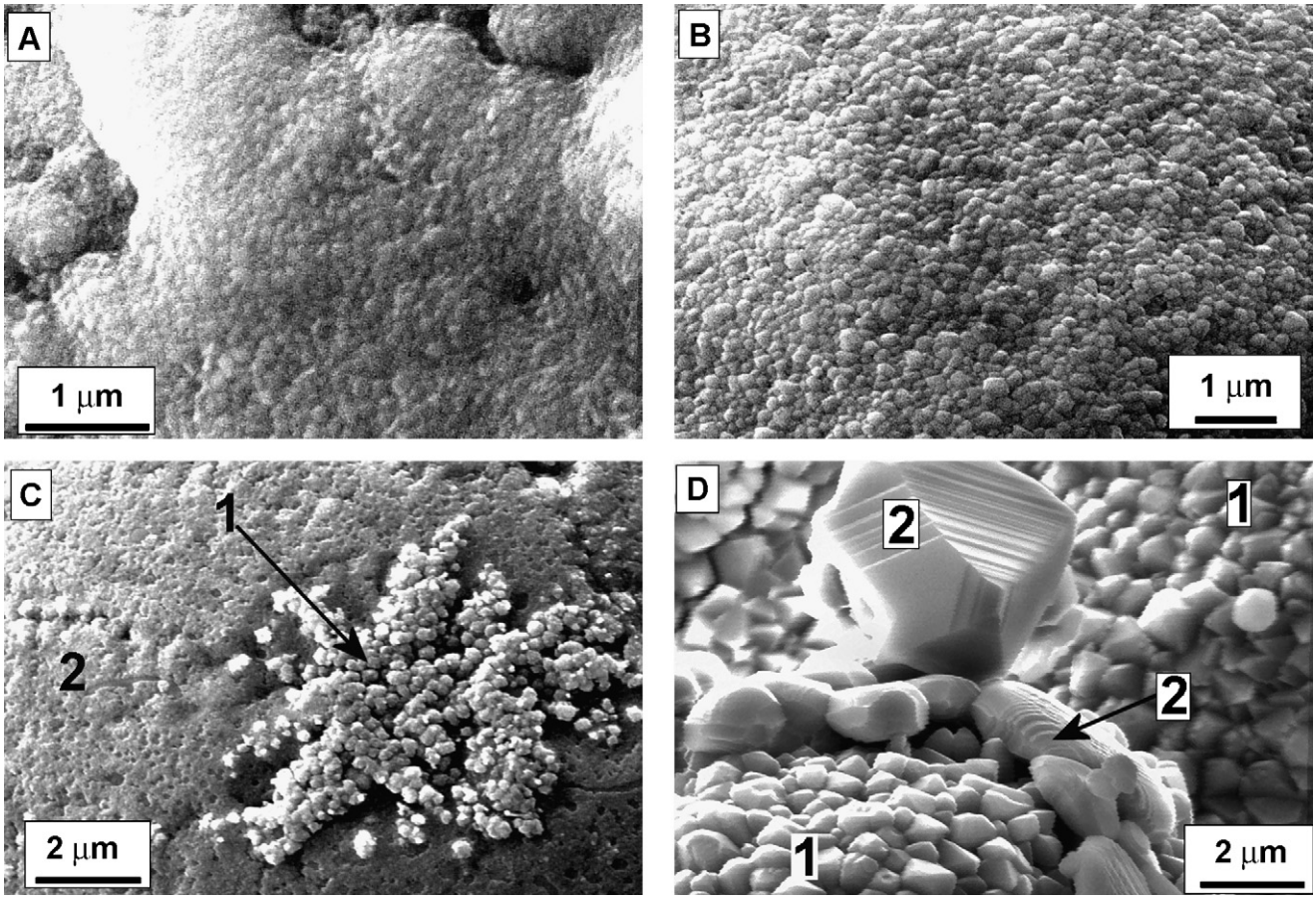

Fig. 5. Spray powders heat treated at the DTA peak temperatures: (A) Co800, 846 °C – 5 min; (B) Co800, 1050 °C – 5 min; (C) Co800, 1146 °C – 5 min (1 = oxide clusters; 2 = damaged surface); (D) Ni700, 1258 °C – 5 min (1 = Ni, Cr oxides; 2 = Ni oxides).

the steel counterbody, wear tracks on as-sprayed Co800 coatings display large damage (SEM micrograph in Fig. 9A). No significant morphological differences exist between wear tracks obtained under different contact conditions. Moreover, a large amount of oxidized material exists inside the wear tracks, as indicated by backscattered electron SEM micrographs (Fig. 9B). EDS analysis indicates that Co, Mo, Cr, Si are the main constituents of these oxides (Fig. 9C). Some transfer material, partly oxidized, may be found on the steel pin (Fig. 9D). Loose wear debris collected on the sample after the test (Fig. 9E) comprises a significant number of rather large metallic debris (with coating composition, as determined from EDS, Fig. 9F) and many smaller, often quite rounded particles. Large damage is also present in the as-sprayed Ni700 wear tracks (Fig. 10A), but the morphology seems different, which indicates that difference in wear mechanisms are likely to exist. In particular, while the Co800 wear track is extremely rough, some smooth areas exist on the Ni700 wear track. Wear mechanisms will be discussed in the following section. Large amounts of oxides (coming partly from the coating and partly from the steel counterbody) are present in this case as well (Fig. 10B and EDS microanalysis in Fig. 10C). Again, a mixture of larger and smaller wear particles exists in the collected loose wear debris (Fig. 10D).

With alumina counterbody, wear tracks display very significant grooving in both cases (Fig. 11A and B), together with some oxide clusters. Grooves are definitely more numerous and sharper for the as-sprayed Ni700 coatings in all contact conditions (compare Fig. 11A and B). In all cases, the wear debris

Table 7
Scratch tests results

Coating	Lc1 (N)	Lc2 (N)	A_g (μm^2)	A_p (μm^2)	A_p/A_g (%)
Co800 (as-sprayed)	4.59 ± 0.98	18.13 ± 0.76	54.7	32.3	59.0
Ni700 (as-sprayed)	2.51 ± 0.01	10.39 ± 1.52	77.6	20.1	25.9
Co800 (heat-treated)	4.72 ± 0.71	21.99 ± 2.55	24.2	11.6	47.9
Ni700 (heat-treated)	4.14 ± 0.95	19.01 ± 0.04	37.0	7.8	21.1

Lc1, Lc2: Critical load for cracking and side chipping; A_g: cross-sectional groove area in "multi-pass" scratch test; A_p: cross-sectional side pile-up area in "multi-pass" scratch test.

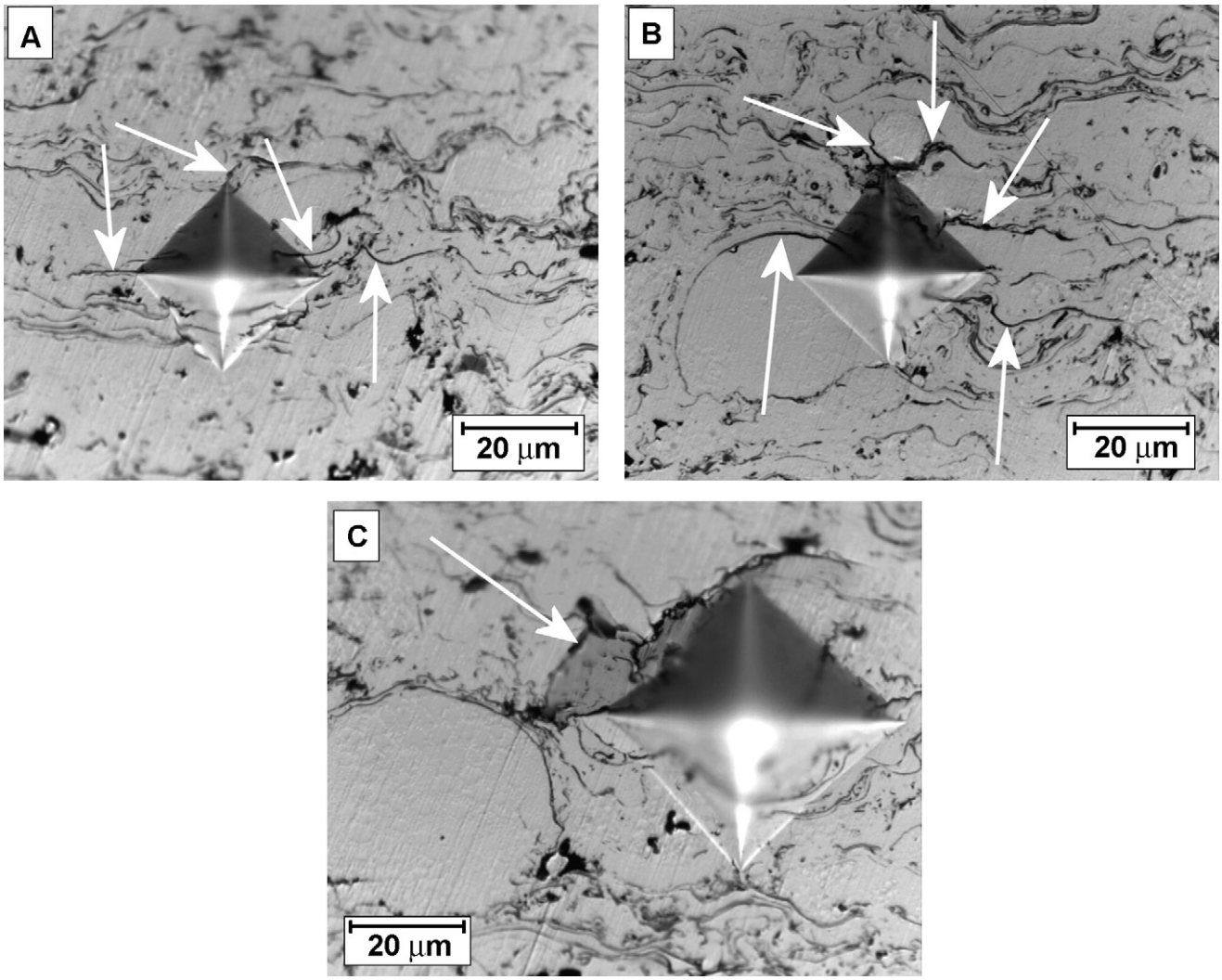

Fig. 6. Vickers microindentations employed for indentation fracture toughness measurement. (A) 5 N indentation on as-sprayed Ni700 coating. Cracks are indicated by arrows. No cracks range out from the lower corner. (B) 5 N indentation on heat-treated Ni700 coating. Cracks are indicated by arrows. Multiple cracking at the top and right corners, and a crack running around an unmolten particle, are noticeable. (C) 10 N indentation on as-sprayed Ni700 coating. The arrow indicates material collapse.

consists in very small, usually oxidized particles (Fig. 11C). The wear tracks on the alumina pin are partly covered by debris (Fig. 11D, areas labelled as 1) and partly bear evidence of brittle intergranular fracture (Fig. 11D, areas labelled as 2).

After the heat treatment, wear resistance of coatings against 100Cr6 steel improves in all cases, particularly for the Co800 one (Fig. 8): its wear rate decreases by two orders of magnitude and is around or lower than 10^{-6} mm^3/(N m). In the highest contact pressure condition (3 mm ball, 10 N normal load), the improvement is lower. A very high improvement is obtained for the Ni700 coating only in the lowest contact pressure condition (6 mm ball, 5 N normal load); in all other cases, the wear rate of heat treated Ni700 exceeds 10^{-6} mm^3/(N m) and increases with increasing contact load. Therefore, coating ranking after heat treatment is reversed: heat treated Co800 outperforms heat treated Ni700 in dry sliding against 100Cr6 in most cases. Except for the highest contact pressure condition, wear tracks on heat-treated Co800 coatings tested against 100Cr6 steel always display little or no damage (Fig. 12A). Some oxides are found on the track; these oxides mainly consist in oxidized steel debris coming from counterbody wear (Fig. 12C). In the highest contact pressure condition, instead, significant damage and much oxidized material are noticeable (Fig. 12B). In this case, the oxidized material mostly contains Co, Mo, Cr, Si, i.e. coating constituents (EDS analysis in Fig. 12D). In any case, the amount of loose debris on the sample was too low to allow collection and observation. Heat treated Ni700 coating wear tracks display evidence some material removal and oxidation (Fig. 13A); oxidized areas mainly contain coating constituents (Fig. 13B). Loose debris consists in quite small particles (Fig. 13C), rather different from those collected on as-sprayed samples.

The wear resistance of heat treated Co800 coating against sintered alumina, instead, does not improve significantly (Fig. 8). Differently from the as-sprayed condition, where the wear rate increases with increasing contact pressure, wear rate of the heat treated Co800 against sintered Al_2O_3 is almost constant in all

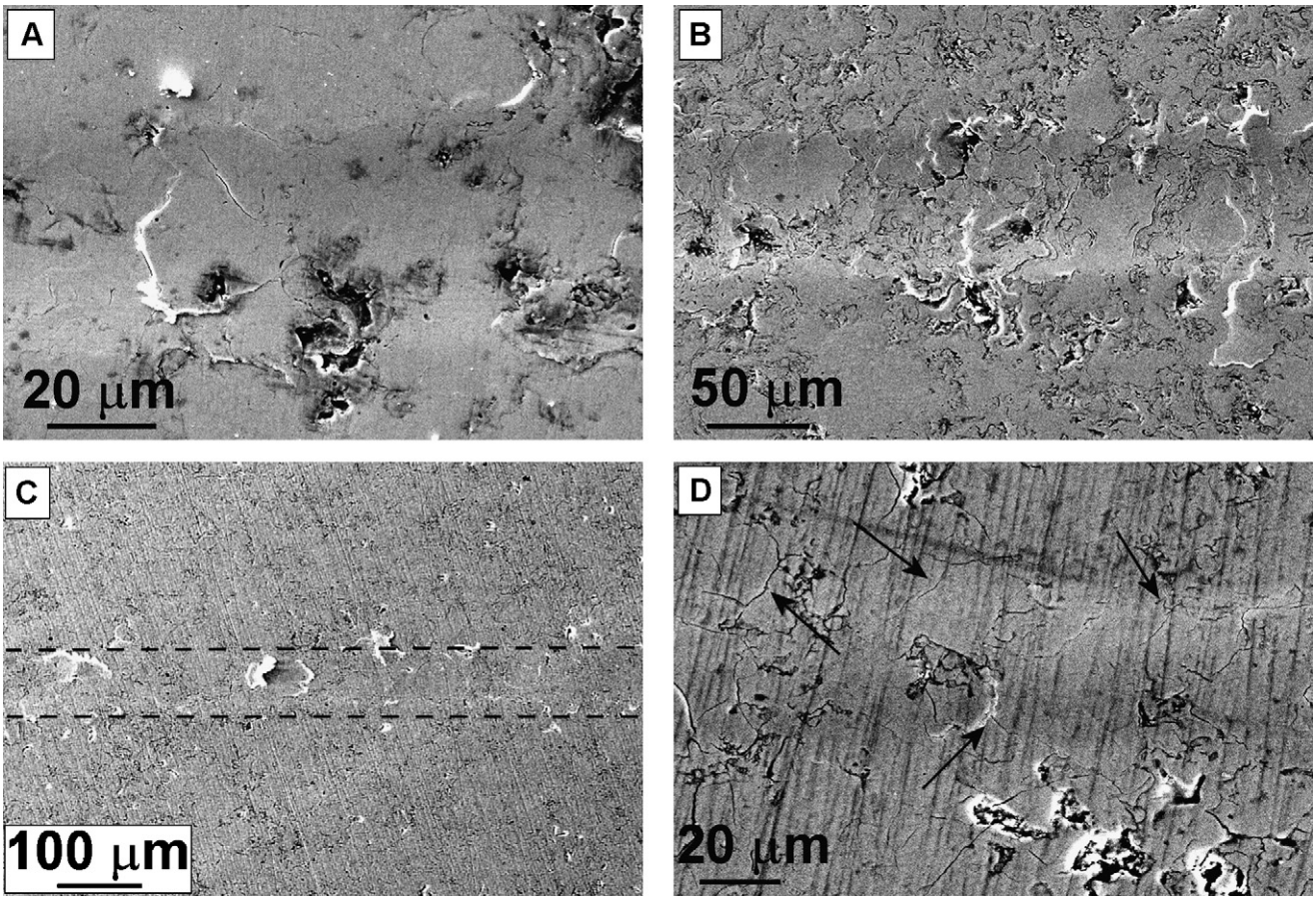

Fig. 7. SEM details of "progressive" scratch tests on as-sprayed Co800 (A), as-sprayed Ni700 (B), heat treated Ni700 (C: dashed line indicates the scratch position), heat treated Co800 (D). Arrows indicate semicircular cracks starting from the groove side.

cases, being around or slightly lower than 2×10^{-5} mm^3/(N m). Again, grooves are noticeable in the wear track (Fig. 14). A moderate improvement is found for the heat treated Ni700; however, its wear rate against Al_2O_3 ball remains higher than the Co800 one, as was the case for as-sprayed coatings, being between 4×10^{-5} mm^3/(N m) and 6×10^{-5} mm^3/(N m) in all cases.

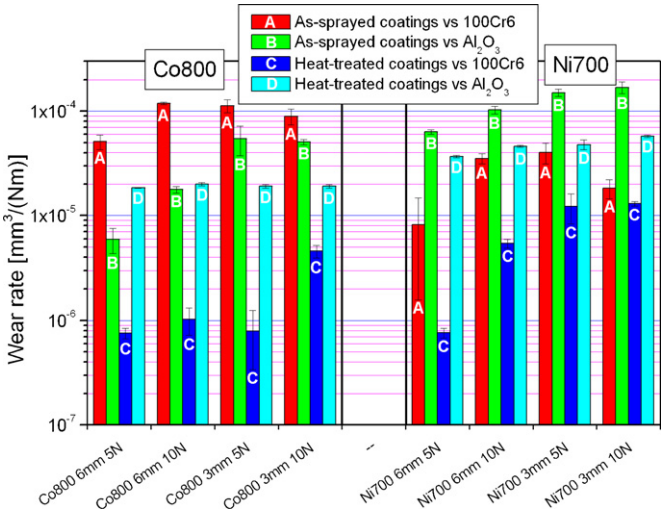

Fig. 8. Coating wear rates recorded after ball-on-disk dry sliding tests.

In all friction curves of as-sprayed and heat treated coatings, two different stages are distinguishable: a first non-stable stage, and a second stage, which is usually (but not always) stable (or quite stable). As-sprayed Co800 coating tested against 100Cr6 steel exhibits, in the first stage, one or more very marked friction peaks, followed by a sudden decrease. In the second stage, the friction coefficient does not reach such high peaks, but is not perfectly stable anyway (Fig. 15A). The initial peak disappears in heat treated Co800 (Fig. 15A). In this case, the friction coefficient gradually increases up to a really stable value, and remains lower than the one recorded for the as-sprayed coating. Similar features are observed with alumina as counterbody (Fig. 15B), but the peak friction coefficient value in the as-sprayed coating is attained after a shorter sliding distance. As-sprayed Ni700 exhibits wide fluctuations in the first stage; in the second, the friction coefficient still oscillates (Fig. 15C). The heat treatment does not prevent initial fluctuations (Fig. 15C), but the second stage friction coefficient is decreased and definitely more stable. With Al_2O_3 counterpart, friction coefficient evolution for as-sprayed Ni700 is similar to that with steel counterpart, displaying initial fluctuations, then a second stage with oscillations around a stable value (Fig. 15D). After the heat treatment, initial fluctuations are suppressed, but oscillations in the second stage still exist (Fig. 15D). The comparison between all recorded friction coefficients is shown in Fig. 16.

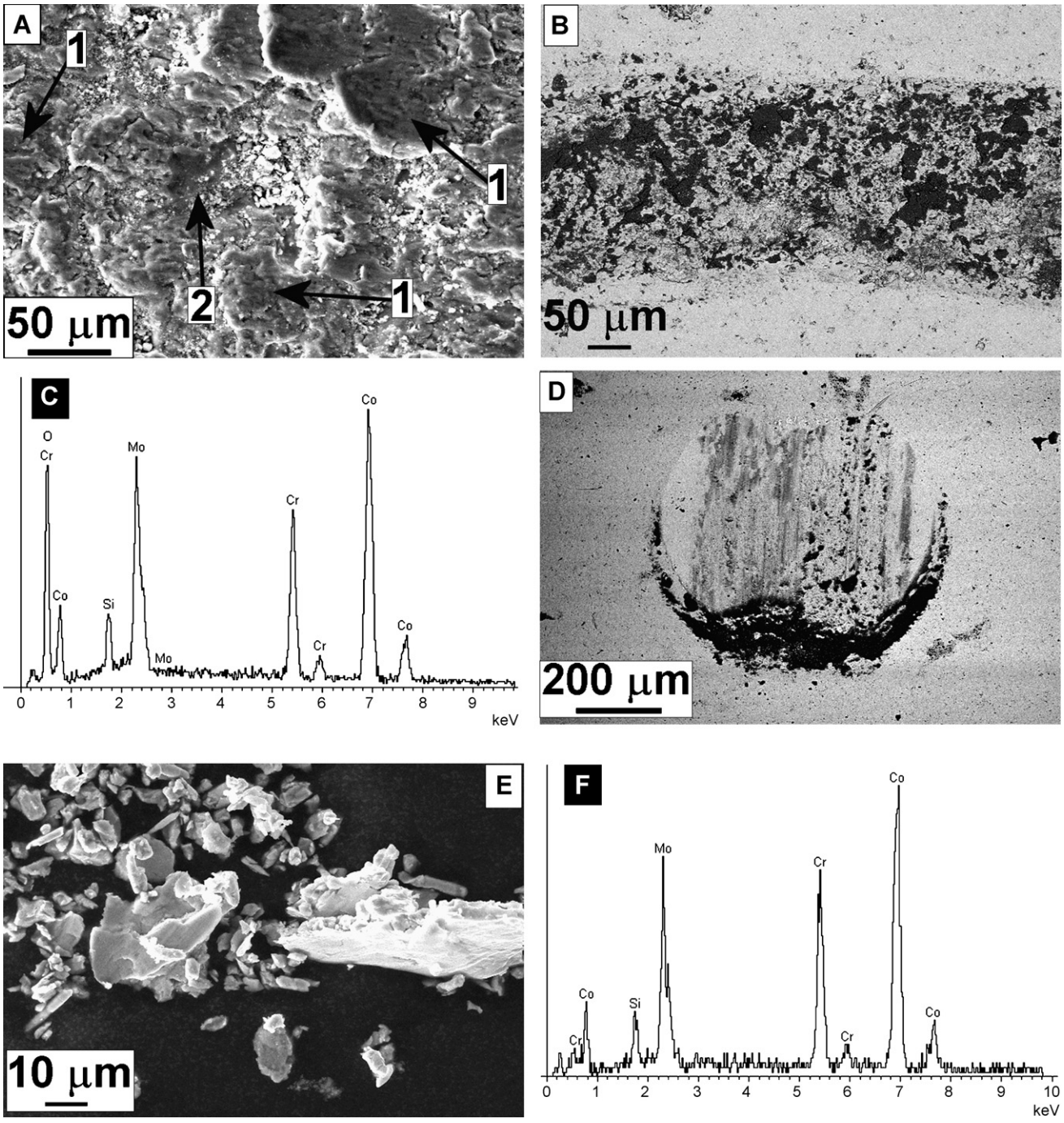

Fig. 9. Tribological tests: as-sprayed Co800 tested against steel pin. (A) Coating wear track, showing evidence of plastic deformation and adhesive wear (1) and of brittle fracture (2); (B) backscattered electron SEM micrograph showing oxide clusters (dark areas); (C) EDS microanalysis of the oxides; (D) SEM micrograph of steel pin with dark oxidized transfer material; (E) wear debris collected after the test; (F) EDS microanalysis of wear debris.

Pin holder position monitoring during the test indicates that, especially for as-sprayed coatings, when peaks or strong fluctuations are present, system wear is faster. Thus, as-sprayed Co800 and Ni700 were tested against 3 mm diameter 100Cr6 ball (10 N normal load) for a 50 m sliding distance to observe the appearance of the wear scar in the first stage of the test. Significant damage is found in both cases (Fig. 17A and B), but no oxide clusters are found. Loose debris consists in large particles, some of which have lamellar morphology (especially for Co800, Fig. 17C).

4. Discussion

First, the discussion will briefly cover the microstructural features of the coatings and the materials thermal behaviour. Then, the wear mechanisms displayed by the coatings tested under the present contact conditions will be analysed. Finally, the significance of the microstructural and mechanical test results will be examined and employed in order to explain the tribological behaviour.

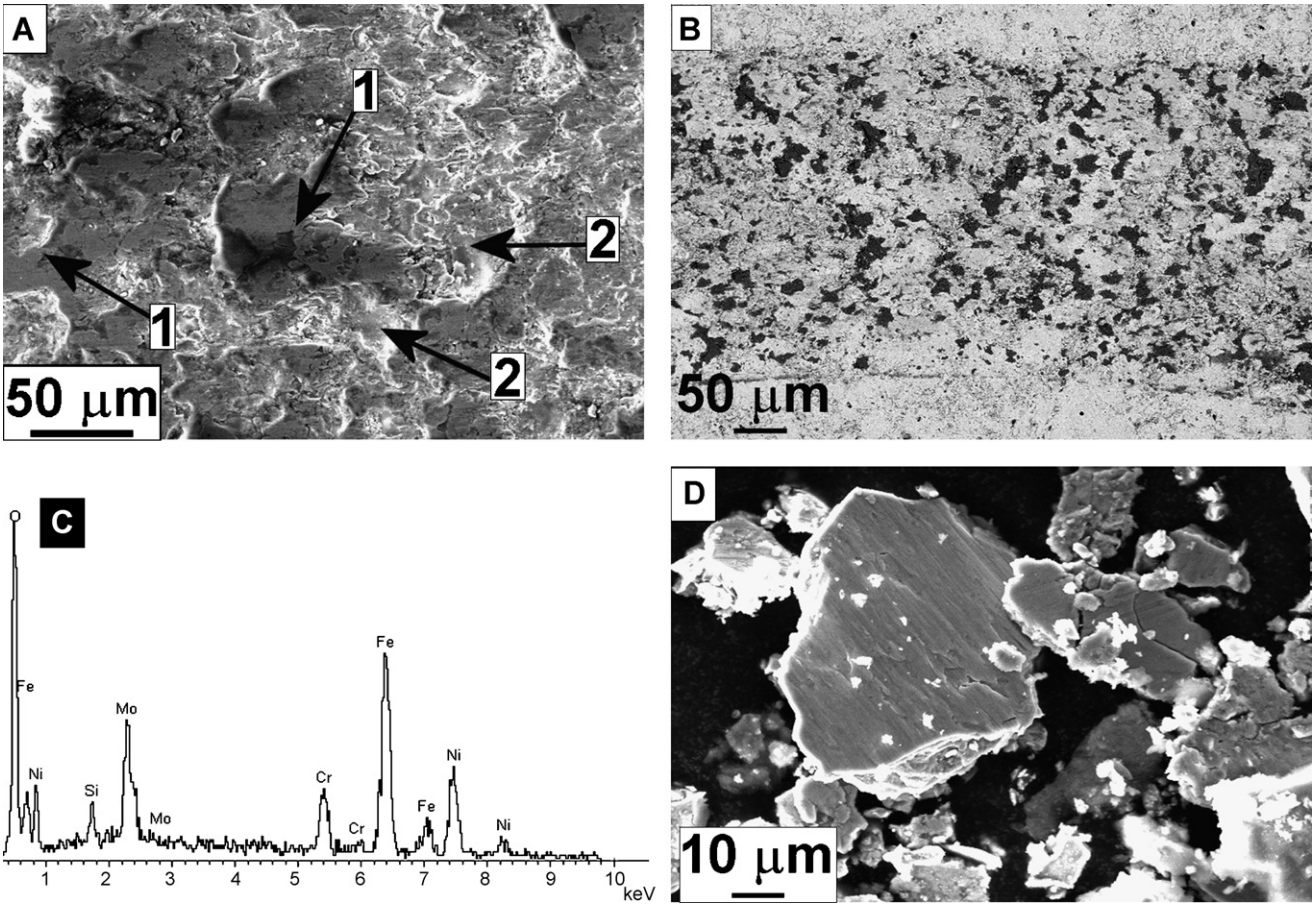

Fig. 10. Tribological tests: as-sprayed Ni700 tested against steel pin. (A) Coating wear track showing smooth areas with limited or no adhesive wear (1) and brittle material detachment (2); (B) backscattered electron SEM micrograph showing oxide clusters (dark areas); (C) EDS microanalysis of the oxides; (D) wear debris.

4.1. Microstructure and thermal behaviour

The large hump which appears in X-ray diffraction patterns at $40^\circ < 2\theta < 50^\circ$ for both coatings (Fig. 3A and B) suggests that the homogeneous metal matrix which is found in most flattened, fully melted splats is mainly amorphous. In these homogeneous areas, indeed, even high-resolution FEG-SEM micrographs cannot highlight any precipitate (Fig. 4A). Crystallization is difficult because of the very high cooling rate of sprayed molten metal droplets upon impact on the substrate (around or higher than 10^5 K/s [26]). Moreover, both alloys contain four elements with significant differences in atomic radii: this condition is known to favour the formation of amorphous phases in metal alloys [27]. Large-sized crystals only exist in unmolten or semimolten particles, which retain the crystalline structure of the original powder (Fig. 2A and B). After the heat treatment, the higher intensity of diffraction peaks implies a higher overall amount of crystalline phases. Indeed, numerous secondary precipitates appear in fully molten splats, which formerly displayed a homogeneous microstructure (Figs. 2C, D, 4B and D). The Sherrer formula has been employed to compare the crystal grain size between as-sprayed and heat treated coatings. The absolute value of the crystal grain size obtained by the simple Sherrer formula cannot be considered reliable, and is probably underestimated, because other factors, such as instrumental line broadening or peak broadening due to microstrains, increase peak width [24]. A precise estimation of the grain size from X-ray diffraction patterns would require the application of more sophisticated pattern fitting techniques [28]. However, the presence of several phases with some overlapping peaks, the existence of very low intensity diffraction peaks, and the overlapping of the amorphous hump (which would be very difficult to subtract from the pattern) may limit results significance or even prevent fitting convergence. For these reasons, only the ratio between grain sizes of heat treated and as-sprayed coatings computed by the Sherrer formula has been presented in this study, whereas FEG-SEM micrographs have been employed for grain size estimation. Both the grain size ratio from Sherrer formula (Table 5) and the grain size estimation from FEG-SEM measurements (Table 4) suggest that no significant increase in grain size occurs, neither for Ni700 not for Co800. Therefore, the heat treatments very largely increased the number of crystals, but not their average size. The formation of a very large number of small, sub-micrometric crystals can be expected to be a very favourable condition for the enhancement of coating mechanical properties and wear resistance.

DTA-TG analyses indicate that both coatings are extremely sensitive to oxidation when temperature exceeds a critical value. This can result in high reactivity of the heated particles in the HVOF gas jet, which may explain the presence of splat boundary oxide stringers in the coatings (Fig. 1A and B). The oxidation

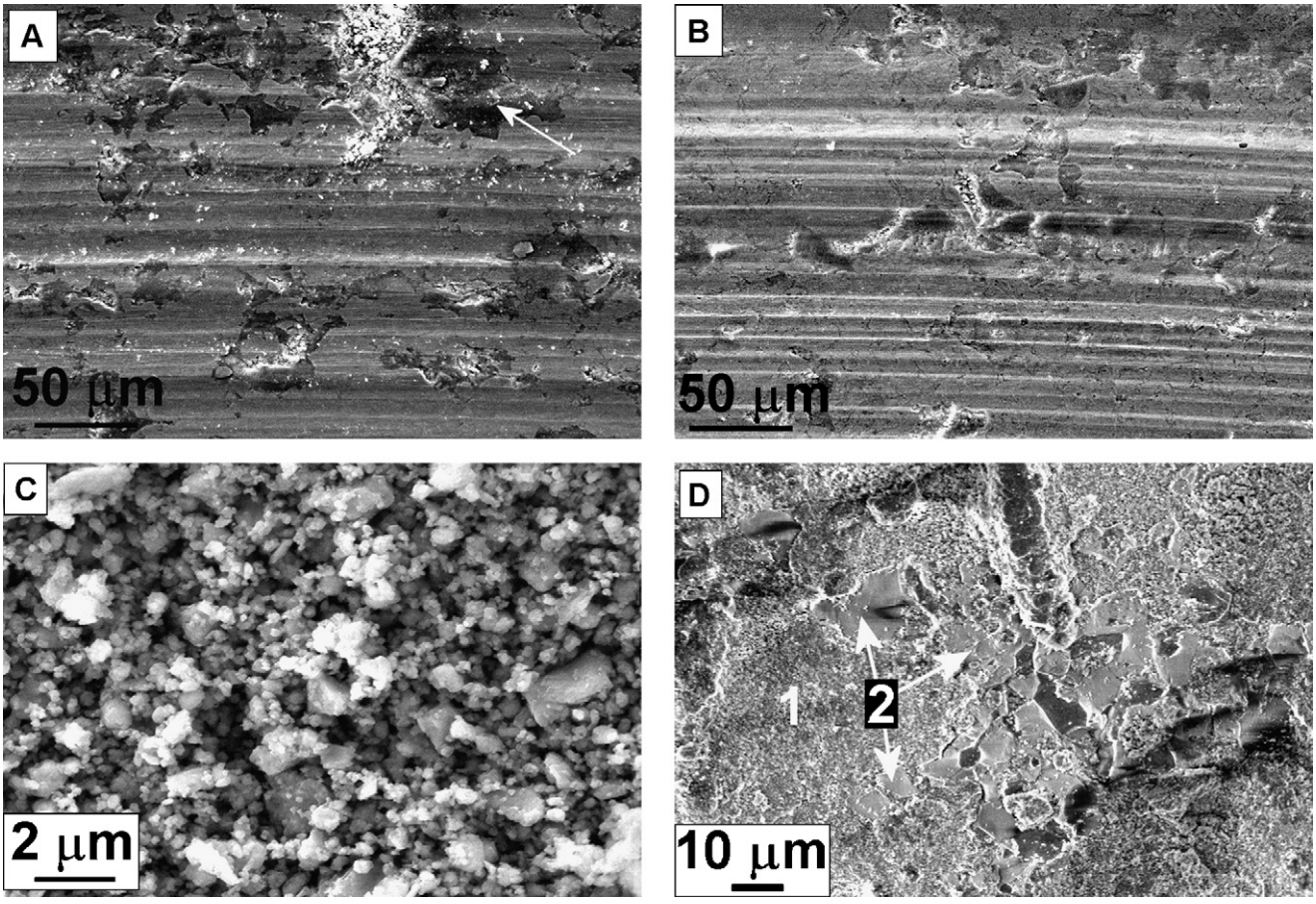

Fig. 11. Tribological tests: as-sprayed coatings tested against Al_2O_3 pin. (A and B) Wear tracks on Co800 and Ni700 coatings, respectively; (C) wear debris collected on Ni700 sample; (D) Al_2O_3 pin wear scar: 1 = transfer material from pin; 2 = intergranular brittle fracture.

behaviour of these materials seems different. Co800 displays three different DTA peaks, corresponding to three different oxide layer morphologies on treated powder particles. It is likely that the powders, from room temperature up to the onset of the first DTA peak, are covered by a very thin, dense and thermodynamically stable oxide layer, probably based on Cr_2O_3. When temperature increases, this layer may become unstable: indeed, oxidation of Cr^{3+} to Cr^{6+} is known to occur at temperatures around or higher than 800 °C, resulting in the oxide layer losing its protective effectiveness [29]. The oxide layer found at the temperature of the first DTA peak (846 °C) contains all coating elements (Fig. 5A, Table 5), even though, compared to the base alloy composition, it is definitely enriched in Cr, but also in Mo. It must always be reminded that chemical analysis by EDS technique can only be regarded as semi-quantitative, due to its limited sensitivity and accuracy. Moreover, the depth of the X-ray generation region may exceed the layer thickness and involve the underlying metallic material as well. Much more accurate chemical and structural analyses are required to clearly define the nature of these compounds, but such study would be out of the aims of the present paper. At the second DTA peak temperature (1050 °C), a completely different layer, with larger grains, is found (Fig. 5B). It almost exclusively contains Cr and O (Table 5), indicating that a completely different compound has become thermodynamically stable in this temperature range. The Cr weight percentage (51%) is very close to that in the CrO_3 compound (52%). This suggests poor stability and low protectiveness of the layer, resulting in continuous oxidation of the underlying material. At the third DTA peak (1146 °C), the surface morphology is deeply affected (Fig. 5C); large-grained oxides appear, containing all alloy elements. Such appearance probably indicates that the oxidation process has become definitely catastrophic. The Ni700 alloy only displays one DTA peak (1258 °C), at higher temperature than Co800, and lower overall weight gain suggesting a slightly higher oxidation resistance. At the peak temperature, a very large-grained oxide layer is found (Fig. 5D), quite clearly consisting in $NiCr_2O_4$ and NiO grains (Fig. 5D and Table 5), which are not protective and grow at a fast rate [30].

4.2. Wear mechanisms

The above listed results indicate very interesting tribological differences between HVOF-sprayed Co800 (Tribaloy-800) and Ni700 (Tribaloy-700) coatings.

Among as-sprayed coatings, the Co800 displays higher wear rates than Ni700 in all sliding tests against 100Cr6 steel.

Co800 wear tracks exhibit damaged metallic areas (Fig. 9A) and oxide clusters (dark areas in Fig. 9B). By observing the damaged metallic zones, two different wear mechanisms appear

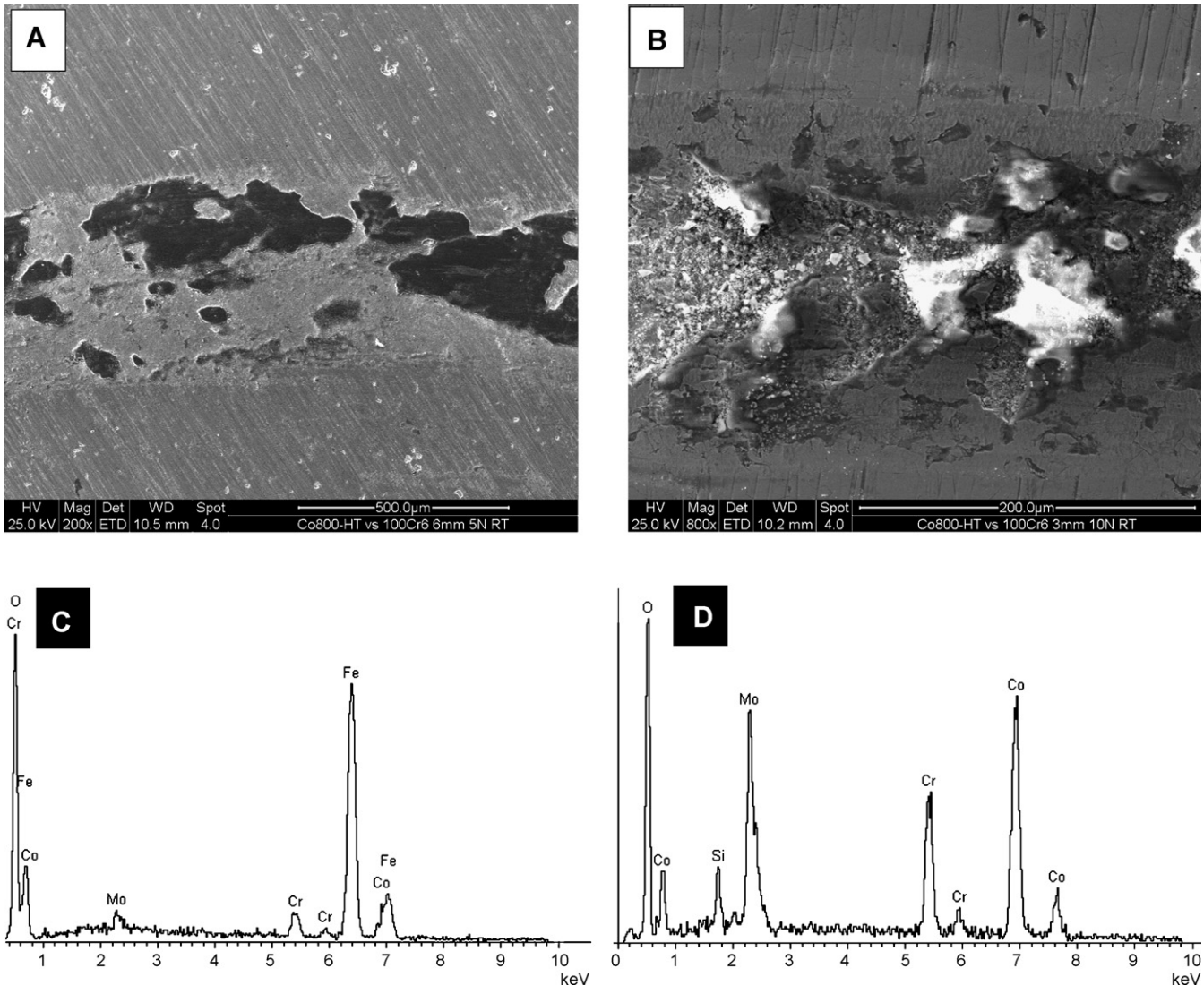

Fig. 12. Tribological tests: heat treated Co800 tested against 100Cr6 pin. (A) Coating wear track, test conditions: 6 mm ball, 5 N load; (B) coating wear track, test conditions: 3 mm ball, 10 N load; (C and D) EDS microanalyses of oxide clusters on wear tracks shown in (A) and (B), respectively.

(Fig. 9A). In some regions of these metallic areas, material loss seems coupled to extensive yielding and plastic shearing (regions labelled as 1 in Fig. 9A). Rounded features and small dips in these regions suggest that the coating material could have adhered to the steel counterpart. Plastic shearing and coating damage could be the consequence of such adhesive process; indeed, literature confirms that plastic shearing of surface material often occurs when adhesive phenomena are taking place [31–33]. The existence of some coating material partly oxidized and transferred to the pin may confirm that adhesion between pin and coating occurred (Fig. 9D). In other regions of the metallic areas, the coating material seems to have been removed by brittle fracture processes, with brittle fracture surfaces being quite clearly visible (Fig. 9A, regions labelled as 2). The large particles found in the wear debris (Fig. 9E) can result either from brittle fracture processes, with cracks initiating below the surface due to the hertzian contact stresses or on the surface due to the tensile stresses caused by the frictional force [23], or from plastic yielding and adhesive wear. In fact, it is assumed that, when adhesion between contacting surfaces occurs, various mechanisms, including shearing of the near-surface material and fatigue due to cyclic plastic yielding, cause the nucleation and propagation of sub-surface micro-cracks resulting in the detachment of platelet-like particles [31–33]. Such particles are indeed found in the wear debris (Fig. 9E), together with smaller, more rounded particles.

After a much shorter sliding distance, the same phenomena are noticeable. Both brittle fracture (Fig. 17A, region labelled as 2) and incipient yielding and plastic deformation, possibly due to adhesion to the steel counterpart (Fig. 17A, region labelled as 1), are already occurring. In this case, the wear debris collected on the sample mostly consists in large, platelet-like particles (Fig. 17C), corroborating the hypothesis that these particles are produced by sub-superficial brittle fracture and extensive plastic yielding. Neither oxide clusters on wear tracks nor smaller, rounded wear debris particles are found after short sliding distances. Therefore, it is likely that oxides (which contain coating constituents rather than Fe from counterpart, Fig. 9C) are formed

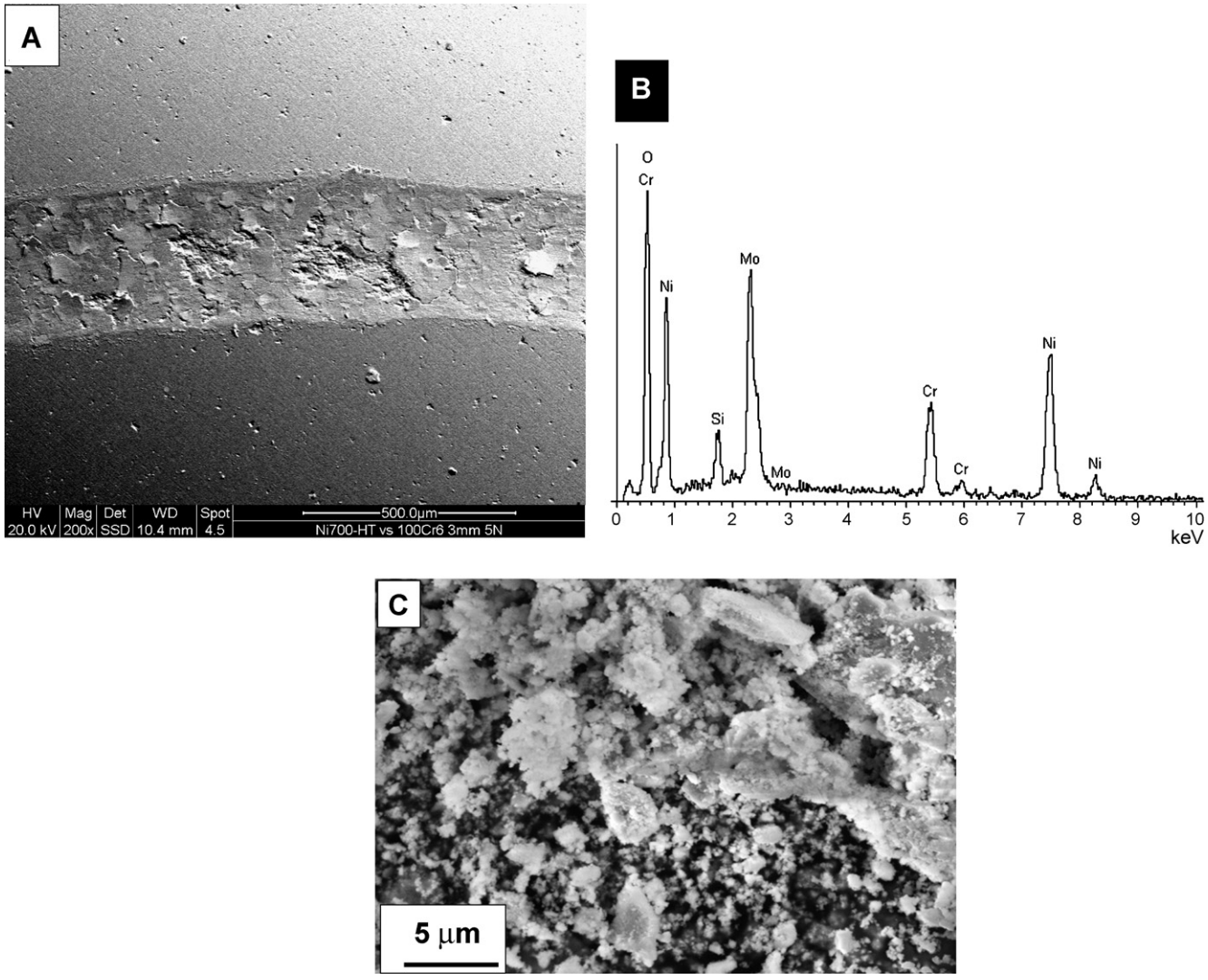

Fig. 13. Tribological tests: heat treated Ni700 tested against 100Cr6 pin. (A) Coating wear track; (B) EDS analysis of oxidized areas; (C) wear debris.

by wear particles trapped in the contact area. They experience repeated yielding, crushing and milling, consequently undergoing progressive reduction in size and strong flash heating [34–36], until they reach a critical oxidation temperature (whose existence is indicated by DTA and TG measurements) and get partly or completely oxidized. Oxidized particles may then stick to the coating surface and form the clusters mentioned above.

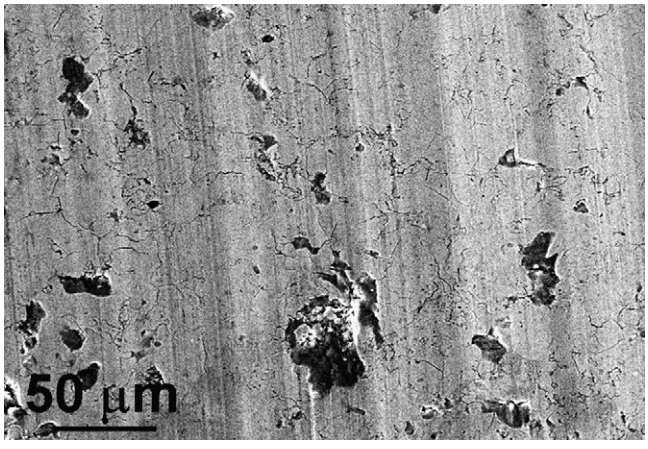

Fig. 14. Tribological tests: wear track for heat treated Co800 after ball-on-disk test against Al_2O_3 pin.

These phenomena can explain the existence of two different stages in the friction curve (Fig. 15A). Indeed, the adhesive phenomena and plastic shearing occurring during metal to metal contact at the beginning of the test definitely increase tangential forces. If some loosely bonded oxides are formed, the friction coefficient can have fluctuations: these oxides reduce adhesion, but are quickly removed from the surface. When a sufficient amount of oxides are formed and firmly sticked onto the coating surface, originating the clusters, direct metal to metal contact is permanently reduced, so that friction is lower in this second stage of the friction curve [36].

The morphology of the wear tracks on the as-sprayed Ni700 coatings tested against steel pin will be now considered. It is different from that of Co800. Smooth regions with limited or no evidence of plastic shearing and adhesive wear are present (Fig. 10A, regions labelled as 1). In other regions, fracture surfaces are present, suggesting that brittle fracture wear is occurring (Fig. 10A, regions labelled as 2). Therefore, one of

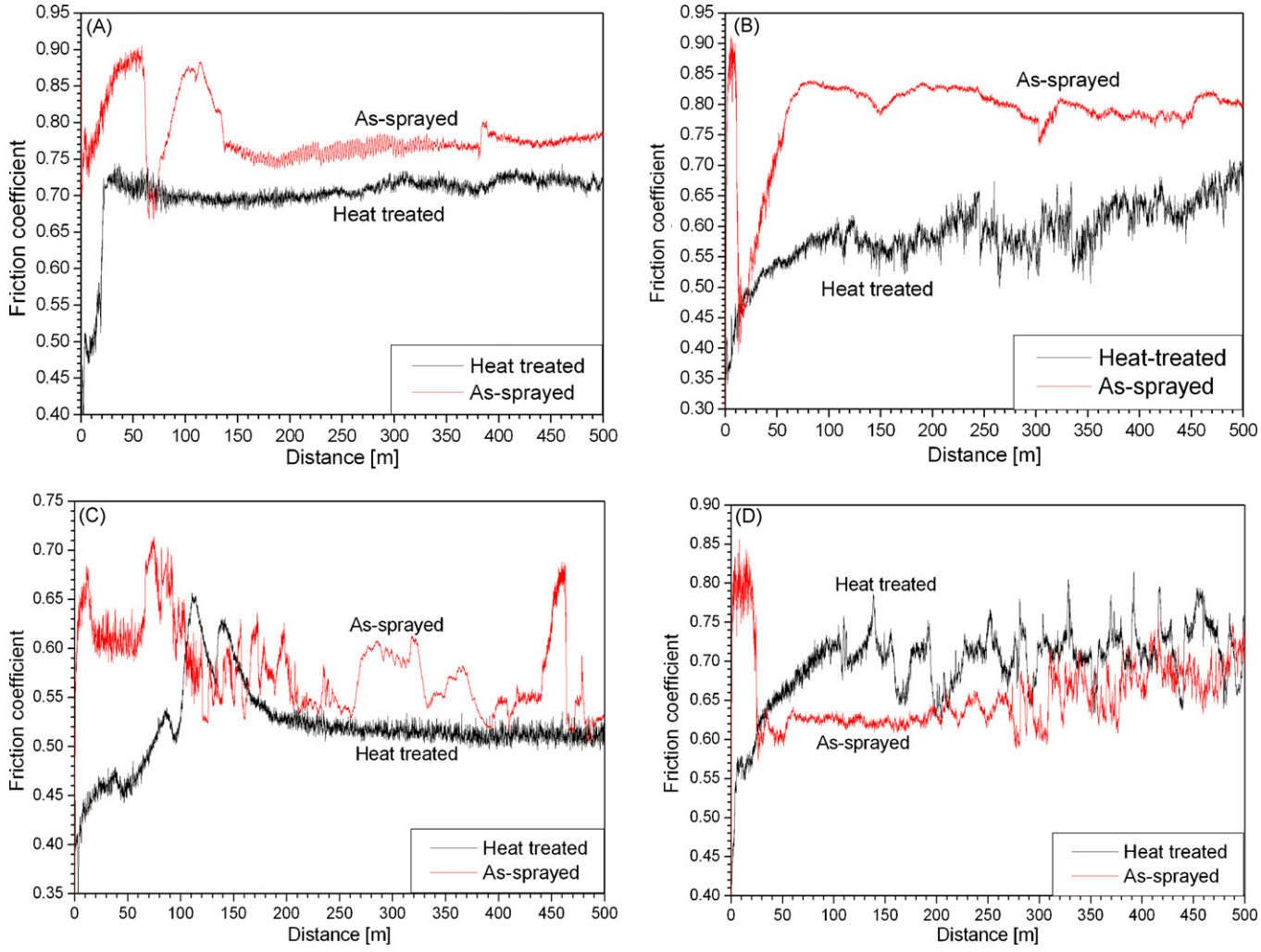

Fig. 15. Friction coefficient curves for as-sprayed and heat treated coatings. (A) As-sprayed and heat treated Co800 against 100Cr6 steel pin (3 mm, 5 N); (B) as-sprayed and heat treated Co800 against Al_2O_3 pin (3 mm, 5 N); (C) as-sprayed and heat treated Ni700 against 100Cr6 steel pin (3 mm, 5 N); (D) as-sprayed and heat treated Ni700 against Al_2O_3 pin (3 mm, 5 N).

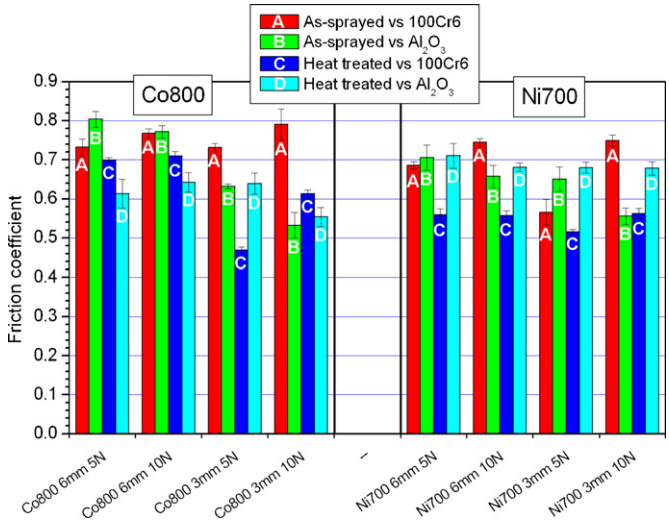

Fig. 16. Average second stage friction coefficient for all tested coatings.

the two wear mechanisms occurring on Co800 sliding against steel, plastic shearing and adhesive wear, is not taking place on Ni700. This explains the lower wear rates for as-sprayed Ni700 compared to Co800. Wear debris collected on Ni700 coatings tested against 100Cr6 steel still contains large particles, resulting from the brittle material detachment, together with smaller particles formed by crushing of the larger particles (Fig. 10D). Brittle fracture processes start almost at the beginning of the test; indeed, regions where material has already been removed by crack propagation (Fig. 17B, region labelled as 2), together with cracks which start propagating along undamaged regions (Fig. 17B, cracks indicated by arrows), are noticeable after 50 m sliding distance. Like for Co800, after such short sliding distance no oxide clusters are found on the wear track. Instead, they appear in the wear track at the end of the test (dark areas in Fig. 10B). It is likely that they are still formed by break up and oxidation of wear debris. However, DTA-TG has shown that Ni700 has a much higher peak oxidation temperature than Co800, the first DTA peak occurring at 1258 °C versus 846 °C for Co800. Moreover, the overall coating wear is lower, thus

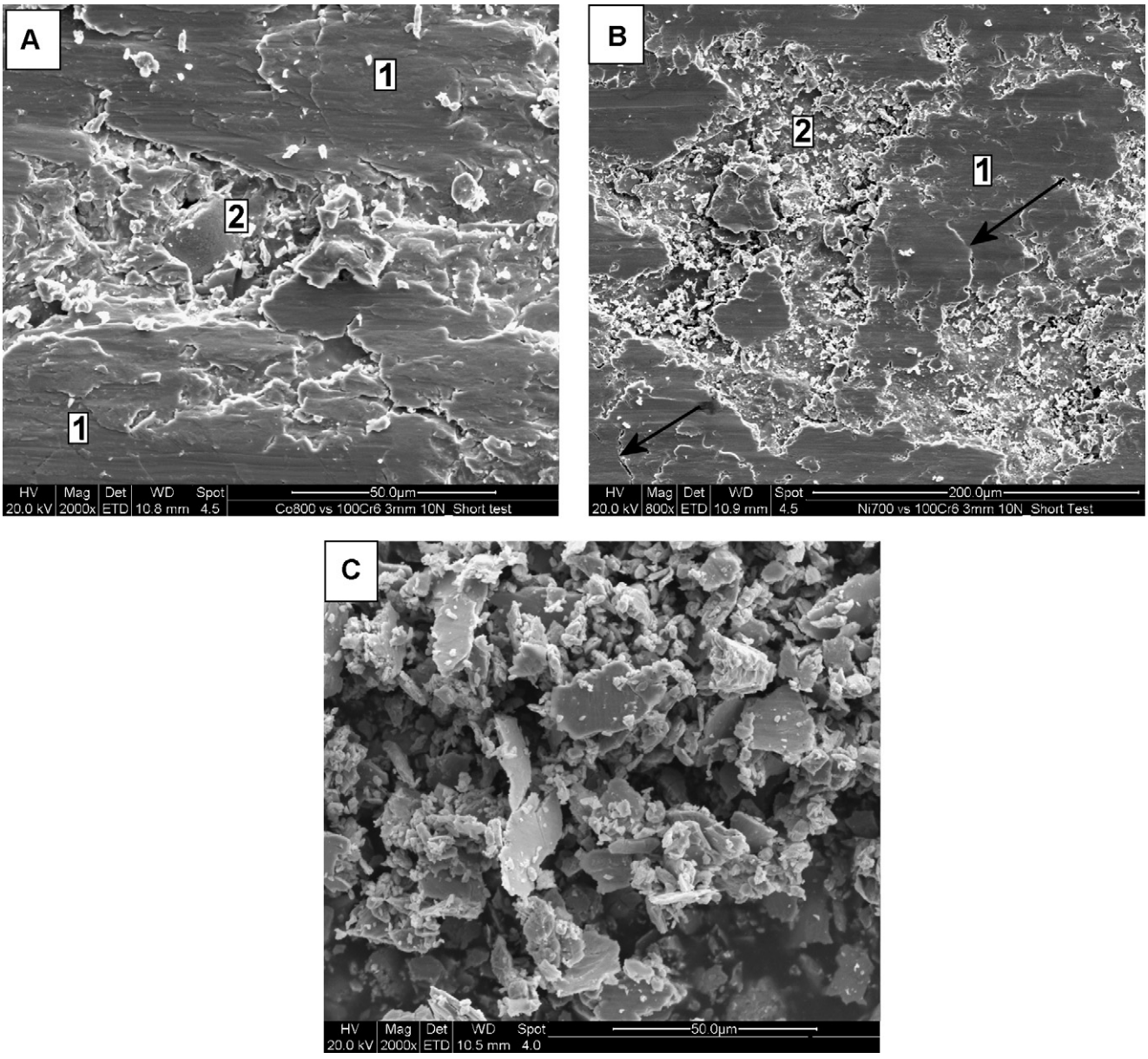

Fig. 17. Tribological tests: as-sprayed coatings tested against steel pin (3 mm pin diameter, 10 N normal load) with shorter sliding distance (50 m). (A) Co800 wear track. 1 = incipient plastic shearing and adhesive wear; 2 = brittle fracture region. (B) Ni700 wear track. 1 = smooth regions with incipient brittle cracking; 2 = brittle fracture region; arrows: cracks which start propagating through smooth regions. (C) Co800 wear debris.

resulting in a lower amount of wear debris from the coating itself. Therefore, the debris coming from the steel counterpart gives a much more significant contribution to the formation of the oxide clusters compared to the Co800 case, explaining the significant amount of Fe now found in these clusters (Fig. 10C).

Once again, the formation of oxide clusters may explain the presence of two different friction stages (Fig. 15C). Large initial fluctuations in the friction coefficient are likely due to the brittle fracture process, generating large wear particles in the contact area and making contact conditions not stable. While for Co800 the plastic shearing and adhesion phenomena resulted in very high friction peaks, no significant adhesive phenomena are found for Ni700, thus resulting in lower peak values of the friction coefficient (compare Fig. 15C and A). When oxide clusters are formed, direct contact between the metallic surfaces is prevented, limiting brittle fracture. Wear still goes on since the film is not uniform (Fig. 10B). Thus, friction oscillations still occur in the second stage.

The ranking between the wear resistance of as-sprayed Ni700 and Co800 coatings is reversed in the tests against Al_2O_3 counterpart (Fig. 8). The much lower chemical compatibility between the ceramic pin and the metallic surfaces implies that adhesive wear is not likely [37]. Instead, abrasive wear mechanism (abrasive grooving) starts to be in action (Fig. 11A and B). Debris particles are much smaller than those formed against steel counterparts: they are possibly originated by phenomena such as microploughing and microcutting (Fig. 11C). The more numerous and much sharper abrasion grooves in the as-sprayed Ni700

coating wear track (Fig. 11A and B) can suggest that as-sprayed Ni700 has lower capability of withstanding abrasive wear.

The alumina pin displays some intergranular brittle fracture (Fig. 11D, regions labelled as 2), and is largely covered by fine wear debris (Fig. 11D, regions labelled as 1) coming from the counterpart.

As described in Section 3.4, coating wear rates against steel counterparts decrease very significantly after the 600 °C heat treatment. On the Co800 wear tracks, neither adhesive wear nor brittle cracking occur any more (Fig. 12A), except for the highest contact pressure condition (3 mm pin diameter, 10 N normal load). Only transferred material from the pin is found on the wear track (darker regions in Fig. 12A) in the low contact pressure test conditions. Instead, under the highest contact pressure condition, brittle fracture occurs, but plastic deformation and adhesive wear are not observed (Fig. 12B). Thus, the wear rate is higher than in other cases. According to the criteria outlined in [9], the wear resistance of heat treated Co800 sliding against the 100Cr6 steel pin can be ranked as "good" or even "excellent" (except for the highest contact pressure condition), being the wear rate around or lower than 10^{-6} mm^3/(N m). Clearly, strengthening of the material due to the heat treatment allowed the suppression of both plastic shearing and brittle cracking, unless the contact pressure is so high that hertzian stresses overcome the material strength. Consistently with the suppression of plastic shearing and adhesive wear, the friction coefficient peak is also suppressed. The friction coefficient attains a truly stable value, lower than in the as-sprayed condition (Fig. 15A).

Heat treated Ni700 exhibits an analogously high wear resistance against 100Cr6 steel counterpart only in the lowest contact pressure condition (6 mm pin diameter, 5 N normal load). The wear rate increases with increasing contact pressure, brittle cracking and delamination being noticeable on the wear tracks (Fig. 13A). Strengthening of the coating after the heat treatment was likely lower than for Co800, so that some brittle fracture processes are still possible, although to a much lower extent than for the as-sprayed coating. Higher stresses due to increased contact pressure thus result in larger cracking and greater wear loss.

Brittle detachment of large wear particles was thought to be responsible for the large friction coefficient fluctuations in the as-sprayed coating. After the heat treatment, the lower occurrence of brittle fracture wear results in much less debris being generated: consistently, friction coefficient fluctuations are reduced and friction is slightly decreased (Figs. 15C and 16).

Al_2O_3 counterbodies still cause abrasive wear (Fig. 14) on both heat treated coating materials. No large change in the wear mechanism seems to have occurred after the heat treatment in this case, explaining the lack of significant improvement of coatings wear resistance (Fig. 7).

4.3. Mechanical properties and explanation of the tribological behaviour

Mechanical properties allow explaining the formerly discussed tribological behaviour. From depth-sensing Vickers indentation it is found that Vickers hardness and elastic modulus increase after the heat treatment, and that, in all cases, they are higher for Co800 than for Ni700 (Table 6). Hardness increase after the heat treatment is consistent with former research [18] and is much likely due to the precipitation of a large number of hard [5,6] and very small crystalline intermetallics, as discussed in Section 4.1. Hardness of a material is generally correlated to its local yield strength [38,39]: hardness increase thus implies higher coating yield strength. Not only Vickers microhardness, but also elastic modulus is significantly increased; in fact, the Laves phases are reported to possess a very high elastic modulus, higher than that of the Co- or Ni-based solid solutions [6].

Besides depth-sensing microindentation, scratch tests also provide useful information. The A_p/A_g percent ratio obtained from "multi-pass" tests, which simulate the repeated sliding of a hard counterpart on the coating surface, can be considered a measure of the coating ability to undergo extensive plastic deformation once contact loads exceed its yield strength. Indeed, contact pressures during scratch testing are normally very high, and will likely exceed yield strength of most metallic materials [40]. An A_p/A_g percent ratio closer to 100% implies that, during indentation, a large portion of the material plastically flows to the side of the groove, thus indicating large plastic deformability. Moreover, such high value can suggest that, during abrasive wear, this material will tend to undergo a less dangerous microploughing wear mechanism [31], where hard counterbody asperities do not directly detach material from the coating, but displace it to the groove sides. A lower percent ratio value indicates limited plastic deformability; this coating may tend to undergo more dangerous abrasive wear mechanisms, like cutting wear, with direct material removal in from of the hard counterpart asperity.

Critical loads from "progressive" scratch tests, especially Lc2, are a measure of the brittleness of the material, and of its tendency to undergo material loss by brittle fracture mechanism.

It is noted that Co800 is, in all cases, more resistant to brittle fracture and more plastically deformable than Ni700. More notably, brittle cracking resistance significantly increases and plastic deformability largely decreases for both coatings after the heat treatment. Higher cracking resistance is consistent with the strengthening effect of the very numerous, small and strong intermetallic crystals formed after the heat treatment. The low plastic deformability of hard intermetallics, such as Laves phases [4,6], can explain the reduction in the plastic deformability after yielding.

Basing on these considerations, the tribological behaviour of the coatings can be interpreted. Indeed, the low hardness (i.e. low yield strength) and high tendency to extensive plastic deformation once yield strength is exceeded both explain the tendency of as-sprayed Co800 to undergo plastic shearing and adhesive wear in dry sliding tests against 100Cr6 steel pin. Moreover, its low cracking resistance (low Lc2) favours material removal by brittle fracture: clearly, the critical cracking load of the coating has been exceeded under all test conditions, causing extensive failure. The high plastic deformability, which is unfavourable in the case of adhesive wear occurring against 100Cr6 steel counterpart, is instead helpful in resisting abrasive wear phenomena against alumina counterpart. Indeed, as discussed above, such plasticity

implies a higher tendency to a less dangerous microploughing wear mechanism.

As-sprayed Ni700 is less hard, less plastically deformable and less resistant to cracking than as-sprayed Co800. Although its lower hardness would suggest a lower resistance to adhesive wear, the significantly lower plastic deformability explains why plastic shearing phenomena are not found for this coating in sliding tests against 100Cr6 steel. Low cracking resistance clearly explains the existence of brittle failures. In tests against alumina, low plastic deformability and low hardness both contribute to a lower abrasive wear resistance than Co800; indeed, plastic deformability after yielding and high hardness are both important for abrasive wear resistance [31,41].

After the heat treatment, much higher hardness and much lower plastic deformability of Co800 coatings explain the disappearance of plastic shearing in tests against 100Cr6 steel. The largely increased cracking resistance implies that brittle cracking can only occur when contact loads are extremely high, as in the case of the highest contact pressure condition. In tests against alumina, the lower plastic deformability causes a higher tendency to a more severe cutting wear mechanism during sliding of hard asperities, thus counterbalancing the positive effect that the hardness increase would have had on abrasive wear resistance. Consequently, no significant increase in wear resistance against the alumina pin is found for the heat treated Co800 coating.

Ni700 also becomes harder, more cracking resistant and less plastically deformable after the heat treatment. Thanks to higher cracking resistance, brittle fracture wear against steel is decreased; however, lower plasticity prevents significant improvements of the resistance to abrasive wear against alumina. Moreover, since hardness, crack resistance and plasticity are lower than those for heat treated Co800, wear resistance of heat treated Ni700 is lower than that of heat treated Co800 in all cases.

A final note concerns indentation fracture toughness. It provides a measure of the resistance of a material to the propagation of brittle fractures, but, unlike "progressive" scratch tests, it seems unable to discern between the presently tested coatings and to explain their relevant tribological differences. Various reasons may contribute to this lack of significance. First of all, the cracking modes occurring in these coatings are definitely different from the ideal crack propagation behaviour which is theoretically necessary for the correct application of indentation fracture toughness models, like the Evans-Wilshaw one employed in this study. Ideally, one clearly visible, straightforward crack should propagate from each indentation mark corner [24,42]. In this case, instead, no cracking from some corners occurs, while others display multiple cracking; sometimes, cracks do not even originate from corners (Fig. 5A–C). Moreover, a very significant scattering in toughness measurements exists, as indicated by the extremely high standard deviation (Table 6), so that the use of these values for quantitative comparisons becomes definitely questionable. Indeed, some authors deem indentation fracture toughness formulae not applicable to thermally sprayed coatings [43]. Besides, in indentation fracture toughness tests, cracks mostly propagate along interlamellar boundaries (a phenomenon well documented in literature [23,43,44]). Thus, this property is important when dealing with wear processes that mainly involve interlamellar detachment [23,44]. However, observation of SEM micrographs has indicated that brittle fractures on the present wear surfaces often do not propagate along interlamellar boundaries. Indeed, splat surfaces are seldom recognizable on fractured areas in wear tracks. Therefore, the cracking mechanism produced by indentation fracture toughness tests is poorly correlated to the actual failure mechanisms in the presently performed tribological tests.

5. Conclusions

The dry sliding wear behaviour of HVOF-sprayed Tribaloy-800 (Co–28%Mo–17%Cr–3%Si) and Tribaloy-700 (Ni–32%Mo–15%Cr–3%Si) coatings, both as deposited and after heat treatment at 600 °C for 1 h, has been studied under different contact conditions and different counterpart materials (100Cr6 steel and sintered Al_2O_3). The wear test results have been interpreted on the basis of microstructural characteristics and mechanical properties. It has been found that:

- As-sprayed Tribaloy-800 has a low degree of crystallinity, with very few secondary hard phases. This results in low hardness, high plastic deformability, and low cracking resistance. In dry sliding tests against 100Cr6 steel counterbodies, low hardness and high plasticity make the coating sensitive to damage by plastic shearing and adhesion; low cracking resistance also results in brittle fracture wear. Indeed, scratch tests indicate the occurrence of critical loads above which brittle material detachment suddenly begins: if contact stresses exceed such critical limit, brittle fracture wear occurs extensively. In dry sliding tests against alumina, abrasive wear mechanisms start being in action. In this case, high plastic deformability results in higher tendency to a less dangerous microploughing wear mechanism, thus compensating the deleterious effects of low hardness and conferring the coating a better wear resistance than against steel.
- As-sprayed Tribaloy-700 also has low crystallinity. It possesses lower hardness and lower plastic deformability than Tribaloy-800, and also displays low cracking resistance. Lower plastic deformability results in almost no plastic shearing and adhesive wear against steel. Thus, one of the two wear mechanisms affecting Tribaloy-800 in sliding tests against steel is suppressed in this case, resulting in a better wear resistance, even though wear rates are still quite high. In tests against alumina, lower plastic deformability and lower hardness result in a definitely worse abrasive wear resistance.
- After the heat treatment, Tribaloy-800 has much higher hardness and cracking resistance, but lower plastic deformability. High hardness and low plastic deformability suppress adhesive wear. High cracking resistance prevents brittle fracture wear, which can only take place when applied contact pressures are extremely high. Thus, the wear rate against 100Cr6 steel pins is decreased by two orders of magnitude, unless for extremely severe contact pressure conditions, and the coating wear resistance thus becomes very good. In abrasive wear con-

ditions against alumina counterparts, a coating with decreased plastic deformability will undergo more severe abrasive processes, like microcutting. This counterbalances the beneficial effects of improved hardness and results in lack of significant wear resistance improvements.

- Heat treated Tribaloy-700 also displays improved hardness and cracking resistance and decreased plastic deformability compared to the as-sprayed one. However, its mechanical properties are always inferior to those of heat treated Tribaloy-800. Its wear resistance against steel is improved compared to the as-sprayed coating, because better cracking resistance decreases the extent of brittle fracture wear; that against alumina does not improve much due to the opposing effects of higher hardness and lower plasticity. However, in all cases, the wear resistance of this coating is poorer than that of heat treated Tribaloy-800.
- Finally, it has been noted that both depth-sensing microindentation (Vickers microhardness, elastic modulus) and scratch test ("progressive" scratch test for cracking resistance assessment, "multi-pass" scratch test for plastic deformability measurement) must be coupled in order to properly explain the tribological behaviour of these coatings under the present contact conditions.

Acknowledgements

The contribution of Mr. Binit Kumar to experimental characterization is gratefully acknowledged. Thanks to Prof. Federica Bondioli for DTA analysis and to Dr. Andrea Tombesi for TG measurement. We gratefully acknowledge ing. Fabrizio Casadei, Mr. Francesco Barulli, and Mr. Carlo Costa, Centro Sviluppo Materiali S.p.A. (Roma, Italy) for coatings manufacturing. Partially supported by PRRIITT (Regione Emilia Romagna), Net-Lab "Surface & Coatings for Advanced Mechanics and Nanomechanics" (SUP&RMAN).

References

[1] T. Bernecki, Surface science, in: J.R. Davis (Ed.), Handbook of Thermal Spray Technology, ASM International, Materials Park, OH, 2004, pp. 14–35.
[2] H. Herman, S. Sampath, R. McCune, Thermal spray: current status and future trends, Mater. Res. Soc. Bull. 25 (7) (2000) 17–25.
[3] V.V. Sobolev, J.M. Guilemany, J. Nutting, High velocity oxy-fuel spraying, Maney for the Institute of Materials, Minerals and Mining, Leeds (2004) 65.
[4] C.T. Liu, J.H. Zhu, M.P. Brady, C.G. McKamey, L.M. Pike, Physical metallurgy and mechanical properties of transition-metal Laves phase alloys, Intermetallics 8 (2000) 1119–1129.
[5] R.D. Schmidt, D.P. Ferriss, New materials resistant to wear and corrosion to 1000 °C, Wear 32 (1975) 279–289.
[6] R. Liu, W. Xu, M.X. Yao, P.C. Patnaik, X.J. Wu, A newly developed Tribaloy alloy with increased ductility, Scripta Materialia 53 (2005) 1351–1355.
[7] C. Navas, M. Cadenas, J.M. Cuetos, J. de Damborenea, Microstructure and sliding wear behaviour of Tribaloy T-800 coatings deposited by laser cladding, Wear 260 (2006) 838–846.
[8] J. Przybylowicz, J. Kusinski, Laser cladding and erosive wear of Co–Mo–Cr–Si coatings, Surface Coat. Technol. 125 (2000) 13–18.
[9] Z.A. Foroulis, Guidelines for the selection of hardfacing alloys for sliding wear resistant applications, Wear 96 (1984) 203–218.
[10] T.A. Wolfla, R.C. Tucker, High temperature wear resistant coatings, Thin Solid Films 53 (1978) 353–364.
[11] M.O. Price, T.A. Wolfla, R.C. Tucker, Some comparative properties of Laves- and carbide-strengthened coatings deposited by plasma or detonation gun, Thin Solid Films 45 (1977) 309–319.
[12] T. Sahraoui, N.-E. Fenineche, G. Montavon, C. Coddet, Alternative to chromium: characteristics and wear behavior of HVOF coatings for gas turbine shafts repair (heavy-duty), J. Mater. Processing Technol. 152 (2004) 43–55.
[13] G. Bolelli, V. Cannillo, L. Lusvarghi, S. Riccò, Mechanical and tribological properties of electrolytic hard chrome and HVOF-sprayed coatings, Surface Coat. Technol. 200 (2006) 2995–3009.
[14] D.E. Crawmer, Thermal spray processes, in: J.R. Davis (Ed.), Handbook of Thermal Spray Technology, ASM International, Materials Park, OH, 2004, pp. 54–76.
[15] T. Sahraoui, H.I. Feraoun, N. Fenineche, G. Montavon, H. Aourag, C. Coddet, HVOF-sprayed Tribaloy-400: microstructure and first principle calculations, Mater. Lett. 58 (2004) 2433–2436.
[16] G. Xiao-Xi, H. Zhang, HVOF-sprayed Tribaloy (T-800): microstructure and particle-erosion behaviour, in: C.C. Berndt (Ed.), Thermal Spray: International Advances in Coatings Technology, ASM International, Materials Park, OH, USA, 1992, pp. 729–734.
[17] U.S. Hard Chrome Alternatives Team (HCAT), Joint Group on Pollution Prevention (JG-PP) and Canadian Hard Chrome Alternatives Team (C-HCAT), "Validation of WC-Co, WC-Co-Cr HVOF or Tribaloy 800 thermal spray coatings as a replacement for hard chrome plating on C-2/E-2/P-3 and C-130 propeller hubs and low pitch stop lever sleeve", Joint Test Protocol, 17 November 1999, available upon request.
[18] G. Bolelli, L. Lusvarghi, Heat treatment effects on the tribological performance of HVOF-sprayed Co-Mo-Cr-Si coatings, J. Thermal Spray Technol. 15 (2006) 802–810.
[19] R.N. Johnson, D.G. Farwick, Friction, wear and corrosion of Laves-hardened nickel alloy hardsurfacing in sodium, Thin Solid Films 53 (1978) 365–373.
[20] Deloro-Stellite web site, http://www.stellite.com.
[21] W.C. Oliver, G.M. Pharr, An improved technique for determining hardness and elastic modulus using load and displacement sensing indentation experiments, J. Mater. Res. 7 (1992) 1564–1583.
[22] A.F. Evans, T.R. Wilshaw, Quasi-static solid particle damage in brittle solids—I. Observations analysis and implications, Acta Metallurgica 24 (1976) 939–956.
[23] M.M. Lima, C. Godoy, P.J. Modenesi, J.C. Avelar-Batista, A. Davison, A. Matthews, Coating fracture toughness determined by Vickers indentation: an important parameter in cavitation erosion resistance of WC–Co thermally sprayed coatings, Surface Coat. Technol. 177-178 (2004) 489–496.
[24] B.E. Warren, X-ray Diffraction, Dover Publications Inc, New York, USA, 1990, pp. 251–254.
[25] N. Dragoe, PowderV2: a suite of applications for powder X-ray diffraction calculations programs, J. Appl. Crystallogr. 34 (2001) 535.
[26] D.E. Crawmer, Coating structures, properties and materials, in: J.R. Davis (Ed.), Handbook of Thermal Spray Technology, ASM International, Materials Park, OH, 2004, pp. 47–53.
[27] W.H. Wang, C. Dong, C.H. Shek, Bulk metallic glasses, Mater. Sci. Eng. R44 (2004) 45–89.
[28] Y.H. Dong, P. Scardi, MarqX: a new program for whole-powder-pattern fitting, J. Appl. Crystallogr. 33 (2000) 184–189.
[29] D. Klarstrom, K. Srivastava, Nickel alloys resist high-temperature corrosion, Adv. Mater. Processes 164 (3) (2006) 31–34.
[30] W.R. Chen, X. Wu, B.R. Marple, P.C. Patnaik, Oxidation and crack nucleation/growth in an air-plasma-sprayed thermal barrier coating with NiCrAlY bond coat, Surface Coat. Technol. 197 (2005) 109–115.
[31] B. Bhushan, Principles and Applications of Tribology, J. Wiley & Sons, New York, USA, 1999, pp. 479–585.
[32] G. Straffelini, Attrito e usura: metodologie di progettazione e controllo, Tecniche Nuove, Milano, Italy, 2005, p. 174 (in Italian).
[33] G.W. Stachowiak, A.W. Batchelor, Engineering Tribology, Second ed., Butterworth-Heinemann, Boston, USA, 2001, pp. 533–552.

[34] B. Bhushan, Principles and Applications of Tribology, J. Wiley & Sons, New York, USA, 1999, pp. 431–478.
[35] M.F. Ashby, J. Abulawi, H.S. Kong, Temperature maps for frictional heating in dry sliding, Tribol. Trans. 34 (4) (1991) 577–587.
[36] G.W. Stachowiak, A.W. Batchelor, Engineering Tribology, Second ed., Butterworth-Heinemann, Boston, USA, 2001, pp. 553–570.
[37] B. Bhushan, Principles and Applications of Tribology, J. Wiley & Sons, New York, USA, 1999, p. 304.
[38] D. Tabor, Hardness of Metals, Clarendon Press, Oxford, UK, 1951.
[39] B. Bhushan, Principles and Applications of Tribology, J. Wiley & Sons, New York, USA, 1999, pp. 198–293.
[40] K. Holmberg, A. Laukkanen, H. Ronkainen, K. Wallin, S. Varjus, J. Koskinen, Tribological contact analysis of a rigid ball sliding on a hard coated surface. Part I: Modelling stresses and strains, Surface Coat. Technol. 200 (2006) 3793–3809.
[41] G.W. Stachowiak, A.W. Batchelor, Engineering Tribology, Second ed., Butterworth-Heinemann, Boston, USA, 2001, pp. 483–509.
[42] C.B. Ponton, R.D. Rawlings, Vickers indentation fracture toughness test. Part 1: Review of literature and formulation of standardised indentation toughness equations, Mater. Sci. Technol. 5 (1989) 865–872.
[43] H. Luo, D. Goberman, L. Shaw, M. Gell, Indentation fracture behavior of plasma-sprayed nanostructured Al_2O_3-13 wt.%TiO_2 coatings, Mater. Sci. Eng. A 346 (2003) 237–245.
[44] G. Bolelli, V. Cannillo, L. Lusvarghi, T. Manfredini, Wear behaviour of thermally sprayed ceramic oxide coatings, Wear 261 (2006) 1298–1315.